AD-A039 550 GENERAL MOTORS CORP INDIANAPOLIS IND DETROIT DIESEL --ETC F/G 20/4
RESEARCH ON AEROELASTIC PHENOMENA IN AIRFOIL CASCADES. AN EXPER--ETC(U)
DEC 76 S FLEETER, R E RIFFEL N00014-72-C-0351
UNCLASSIFIED DDA-EDR-9028 NL

| OF |
AD
AD39550

END
DATE
FILMED
6-77

EDR 9028

# RESEARCH ON AEROELASTIC PHENOMENA IN AIRFOIL CASCADES

## An Experimental Investigation of the Unsteady Aerodynamics of a Controlled Oscillating MCA Airfoil Cascade

## Cascades and Flow Systems Research

SANFORD FLEETER
RONALD E. RIFFEL



DECEMBER 1976

Research Supported in Part by
Office of Naval Research
Power Branch
Under Contract N00014-72-C-0351



Detroit Diesel Allison
Division of General Motors Corporation
Indianapolis, Indiana 46206

# An Experimental Investigation of the Unsteady Aerodynamics of a Controlled Oscillating MCA Airfoil Cascade

SANFORD FLEETER
RONALD E. RIFFEL

DECEMBER 1976

Research Supported in Part by
Office of Naval Research
Power Branch
Under Contract N00014-72-C-0351



Detroit Diesel Allison
Division of General Motors Corporation
Indianapolis, Indiana 46206



See 1473

EDR 9028



019200

AB

TABLE OF CONTENTS

## LIST OF TABLES

LIST OF FIGURES

LIST OF FIGURES (Cont.)

LIST OF FIGURES (Cont.)

LIST OF FIGURES (Cont.)

LIST OF FIGURES (Cont.)

## ABSTRACT

A unique unsteady cascade experiment directed at providing fundamental aerodynamic data needed to verify or direct refinements to the basic model of unstalled supersonic torsional flutter in turbomachines is presented. In particular, the steady, quasi-static, and unsteady aerodynamics were determined for a multiple circular arc (MCA) airfoil cascade which modeled the tip section of an advanced design fan blade. The steady airfoil surface aerodynamic performance of the cascade was measured at two levels of aerodynamic loading and correlated with the predictions from a time-marching, steady, transonic flow analysis. The chordwise distribution of the quasi-static unsteady pressure coefficient for a 0° interblade phase angle was then determined and correlated with two appropriate predictions: one based on the steady transonic analysis and the other on steady inviscid supersonic flat plate theory. Finally, the MCA cascade was harmonically oscillated in the torsional mode at a reduced frequency value of 0.14. The fundamental unsteady aerodynamic data was then obtained at a Mach number equal to 1.55 over a range of interblade phase angles for two values of the cascade static pressure ratio. These unsteady results were then correlated with the predictions from state-of-the-art unsteady flat plate cascade analyses.

# INTRODUCTION

The demand for increased engine performance, while maintaining a minimum weight, has taken the compressor designer into flow regimes wherein he has no apriori experience. These advanced design fans and compressors have encountered unstalled supersonic flutter at the design operating condition, that current flutter prediction systems, based on empirical correlations of prior engine aerodynamic flutter data, are inadequate for the task of extrapolating these past experiences, to the new high speed designs. Thus, the need for a phenomenological modeling approach to the development of a well-founded flutter design system, substantiated by key critical experiments which model the fundamental unsteady aerodynamic phenomena, is clearly evident.

The generally used flow model for unstalled supersonic flutter is that of inviscid flow through a compressor stage of differential radial height, which is developed into a two-dimensional rectilinear cascade. The airfoils are assumed to be zero thickness flat plates which are harmonically oscillating in the torsional mode. Even with this simplified model, the problem is still very complex, particularly as the flow involves a subsonic axial velocity component.

Recently, a number of solutions to this basic model involving various mathematical techniques have been developed, as noted and discussed in Reference 1. For the designer to make use of these solutions in a quantitative predictive design system, it is necessary to determine the validity of the mathematical assumptions and to extend the model to more realistic airfoil configurations. To accomplish this, however, fundamental experimental aerodynamic data is needed to verify the model and to further the understanding of the basic unsteady flow physics.

The results of an experimental investigation of the fundamental unsteady aerodynamics associated with an harmonically oscillating airfoil cascade which closely simulates that of the analytical model are presented in Reference 2. The correlation of the experimental data with an appropriate theory is excellent, thereby indicating the validity of the experimental techniques, and the data acquisition and analysis procedures.

The present work is directed at the experimental investigation of an aerodynamic configuration which more closely resembles the physical and aerodynamic conditions of an advanced design rotor blade, including the aerodynamic loading. In particular, the steady, quasi-static, and unsteady

aerodynamics are determined for a multiple circular arc (MCA) airfoil cascade which models the tip section of an advanced design fan blade at two levels of aerodynamic loading. All of the experimental results are correlated with appropriate predictions obtained from state-of-the-art analyses.

## AIRFOIL CASCADE AND INSTRUMENTATION

The two-dimensional cascade utilized in this investigation is comprised of five double-trunnioned steel airfoils modeled from the tip section of an advanced design fan blade. These airfoils are characterized by a 3.00 inch (7.62 cm) span, 2.50 inch (6.35 cm) chord and a 0.075 inch (0.19 cm) maximum thickness at the 50% chord location. The cascade physical parameters are noted in Table I. The airfoil profile is of multiple circular arc (MCA) design with the airfoil coordinates presented in Table II.

The airfoil mounting arrangement in the cascade is shown schematically in Figure 1. An array of torsional frequencies are provided by attaching various thickness spring bars to the trunnions. The double-trunnion airfoils and spring bar assemblies are mounted in plexiglas wind tunnel test section

walls, thereby permitting schlieren flow visualization. Driving arms are attached to the airfoil trunnions which are in turn driven by electromagnets controlled by an on-line computer system, as described in References 2 and 3. In this manner, the torsional frequency of the airfoils and the interblade phase angle are precisely controlled. Strain gages mounted on the spring bars exhibit excellent sensitivity to the torsional movement of the airfoil, and allow measured strain gage signals to be converted to rotational amplitudes.

The choice of proper steady-state aerodynamic instrumentation is important to quantitatively determine the details of the cascade steady flow field. Sidewall static pressure taps were used to establish the cascade inlet and exit pressure distributions. This information combined with schlieren flow visualization was used to establish the steady-state periodicity. In addition, the static pressure distributions on the suction and pressure surfaces of the second and fourth airfoils of the cascade respectively, were measured at the chordwise locations specified in Table II.

The center airfoil (third) of the cascade was machined to permit the chordwise embedding of twelve miniature Kulite LQ series dynamic pressure transducers such that the airfoil

contours were preserved. This was accomplished by placing a thin pliable coating over the transducer diaphragms which resulted in no depreciation in sensitivity. The chordwise transducer locations, presented in Table IV, are schematically indicated in Figure 2. These flush mounted transducers were staggered across the span of each surface, as indicated in Figure 3 which shows a view of the pressure surface.

## EXPERIMENTAL FACILITY

The Detroit Diesel Allison (DDA) rectilinear cascade facility, shown in Figure 4, was conceived and built as a research tool to evaluate the aerodynamic characteristics of compressor and turbine blade sections. The facility is a continuous flow, non-return, pressure-vacuum type wind tunnel with the test section evacuated by means of two primary steam ejectors. Up to 10 lbm/sec of filtered, dried, and temperature-controlled air may be used.

The major features of the facility include the following.

- Continuous operation for extended time periods
- A mechanized test section which permits a cascade of airfoils to be rotated with the tunnel in operation

- A schlieren optical system for visual observation and photography of the test section while the facility is in operation

- A sophisticated instrumentation system centered on a laboratory-size digital computer. The computer provides on-line control of data acquisition, data reduction, and calculates performance parameters while the test is in progress for both steady-state and dynamic testing of airfoil cascades.

In this cascade facility, the entrance flow to the test section is generated by fixed nozzle blocks yielding a Mach number of 1.50. The orientation of a wedge with respect to this nozzle exit flow specifies the test section Mach number, i.e., the shock or expansion wave generated by the wedge determines the cascade inlet conditions.

The wind tunnel facility is completely automated using a dedicated digital computer. For steady-state and/or dynamic investigations, the computer is used for control of instrumentation, data acquisition, and data reduction. The computer and associated peripheral equipment were used in this investigation to:

- Determine the steady-state flow parameters including the inlet Mach number, inlet air density, and instrumented airfoil surface static pressure parameters
- Control cascade excitation such that a torsional mode is imparted to the airfoils at a prescribed frequency and interblade phase angle
- Digitize the time-dependent strain gage and miniaturized high response pressure transducer signals at rates to 100,000 points per second
- Store permanently the cascade steady-state parameters and dynamic data on removable magnetic disks
- Control a dual channel storage oscilloscope to provide an analog record of the time-variant pressure transducer signals
- Control a high speed motion picture camera for schlieren movies of the unsteady phenomena.

## DYNAMIC DATA ACQUISITION AND ANALYSIS

With the tunnel in operation and the airfoil cascade harmonically oscillating at the prescribed frequency and interblade phase angle, the time-variant strain gage and pressure transducer signals were digitized at rates to 100,000 points per second by a 16-channel analog-digital converter and multiplexer system, and stored on a magnetic disk. These digitized data were analyzed on-line to determine the fundamental aerodynamic characteristics of the unsteady phenomena. The parameters of interest are the amplitude of the airfoil motion and the pressure disturbance, the frequency, the interblade phase angle, and the phase difference between the unsteady pressures and the airfoil motion as characterized by the strain gage signal on the dynamically instrumented airfoil, i.e., the pressure phase shift data is referenced to the motion of the dynamically instrumented center airfoil in the cascade.

The amplitude of the airfoil motion and the pressure disturbance is determined by fitting a second order least square function to the data, differentiating it, and evaluating the maximum. The pressure disturbance amplitude is then nondimensionalized into an unsteady pressure coefficient, $C_p$, as defined in Equation 1.

$$C_p = \frac{p}{\frac{1}{2}\rho U^2 \alpha} = \frac{p}{\frac{1}{2}\gamma M^2 p_s \alpha} \qquad (1)$$

where p is the measured unsteady pressure amplitude, $\rho$ is the fluid density, U is the inlet velocity, $\alpha$ is the torsional amplitude of oscillation (in radians), $\gamma$ is the ratio of specific heats, and $p_s$ is the inlet static pressure.

The frequency of the time-dependent data is determined through the autocorrelation function. This function describes the dependence on the values of the data at one time, $X_i$, on the values at another time, $X_{i+r}$. The normalized autocorrelation function, $R_{xr}$, is defined in series form as

$$R_{Xr} = \frac{1}{N-r} \sum_{i=1}^{N-r} X_i X_{i+r} \Big/ \frac{1}{N} \sum_{i=1}^{N} X_i X_i \quad r = 0,1,2...m \qquad (2)$$

where:

$X_i = X(i\Delta t)$

r = lag number

N = total number of dynamic data points

m = number of lags

The lag time, $\Delta t$, is inversely proportional to the rate at which the data is digitized. A typical autocorrelogram of the digitized data exhibits the features of a sine wave plus random noise. A second order least square function is fit to

the data in the second positive peak of the autocorrelogram. The inverse of the time at which this least square function is a maximum is equal to the frequency, f, of the time-dependent data.

The phase difference of the pressure disturbance along the airfoil chord in relation to the airfoil motion is calculated through the cross-correlation function. This function, for two sets of data, $X_i$, $Y_i$, describes the dependence of the values of one set of data on the other. The normalized cross-correlation function, $R_{xyr}$, is defined as:

$$R_{xyr} = \frac{1}{N-r} \sum_{i=1}^{N-r} X_i Y_{i+r} \Big/ \frac{1}{N} \sum_{i=1}^{N} X_i Y_i \quad r = -m, \ldots -1, 0, 1, \ldots m \qquad (3)$$

where the variables are defined analogous to those in Equation (2).

As in the frequency calculation, a second order least square function is fit to the data in the first positive peak of the cross-correlogram. The time, $t_p$, at which this least square function is a maximum is analytically determined. The phase difference, in degrees, is calculated as

$$\theta_p = t_p \, f \, 360 \qquad (4)$$

where f is the frequency calculated for the airfoil motion from the strain gage data, utilizing Equation (2).

Two sources of phase relation discrepancy are inherent in the electronic data acquisition system and correlation computation. The analog-digital (A/D) converter multiplexer unit does not permit data to be digitized simultaneously on all channels. Consequently, an inherent phase shift is introduced into the physical data when the cross-correlation function operates on the raw digitized data. This phase shift, for the sinusoidal data in this experiment, is directly proportional to the "cut rate" of the multiplexer, as shown in Equation (5):

$$\theta_s = f_x(K_y - K_x)\ 350/R_a \qquad (5)$$

where $\theta_s$ is the AD phase shift inherent in the computation between channels $K_y$ and $K_x$, representing the respective data, $Y_i$ and $X_i$. The frequency, $f_x$, corresponds to the disturbance in channel $K_x$, and $R_a$ is the rate at which the data is being digitized.

Prior to acquiring data the electronic data acquisition system is calibrated for phase shift, $\theta_a$, using the AD converter and the computation described in the foregoing. Therefore, the phase difference of the pressure disturbance along the airfoil surface in relation to the airfoil motion is

$$\theta_{xy} = \theta_p - \theta_s - \theta_a \ . \qquad (6)$$

This computational procedure results in a valid on-line data analysis system and provides the experimentalist with meaningful information with which to make judicious decisions during the test. All analyzed results are stored on a magnetic disk for further examination.

## RESULTS

The procedure followed in this experiment included first obtaining a periodic steady-state cascade flow field. This periodicity was determined by means of the schlieren flow visualization and the sidewall static pressure taps located at the leading edge of each of the airfoils in the cascade. The resulting steady-state leading edge static pressure variation of the airfoil cascade was less than $\pm$ 2 percent. Figure 5 is a schematic of the steady-state cascade flow field, determined from the static pressure measurements and the schlieren flow visualization. As indicated, the bow shock intersects the suction surface of the adjacent airfoil near the trailing edge with the shock reflection as well as the adjacent airfoils trailing edge shock intersecting the pressure surface near mid-chord.

With the cascade periodicity established, the steady cascade airfoil surface performance was determined for the aerodynamic conditions of the unsteady experiments. These conditions are

characterized by a 1.55 cascade inlet Mach number value and 1.05:1 and 1.30:1 static pressure ratios. The airfoil surface performance data for these conditions are presented in Figures 6 and 7, respectively. Also presented are the predictions of the steady-state cascade aerodynamic performance obtained from the transonic, time-marching, steady flow analysis of Reference 3. This analysis considers the time-dependent Navier-Stokes equations in conservation-law form which allows for viscous shock wave formation. As can be seen from these figures, the steady aerodynamic loading of the cascade is taken up by the trailing edge shock system, as characterized by the absence of any effects due to the increased loading indicated over: (1) the leading 42% of the pressure surface; (2) the entire suction surface. Overall the airfoil steady surface pressure distribution data correlates very well with the predictions from the transonic flow analysis. The correlation is not as good near to the leading and trailing edges, regions where the analysis does not accurately model the profile of the airfoil. Also, it should be noted that the current state-of-the-art inviscid unsteady flutter aerodynamic model assumes a uniform steady flow field with small perturbations generated by the harmonic oscillations of zero thickness flat plate cascaded airfoils, as previously discussed. Figures 6 and 7 demonstrate clearly the differences between this uniform steady flow of the model and the actual steady flow field.

Prior to oscillating the cascade, a quasi-static experiment was undertaken to obtain the zero frequency limit of the unsteady pressure coefficient for an interblade phase angle value equal to zero degrees. This was accomplished by measuring the airfoil surface static pressure distributions with the cascaded airfoils in their nominal position. The airfoils were then rotated and locked into a position corresponding to that 180° later in the 0° interblade phase angle oscillation, and the resulting static pressure distributions measured. This permitted the chordwise distribution of the quasi-static unsteady pressure coefficient to be determined for each airfoil surface. These results were then correlated with a quasi-static prediction based on inviscid supersonic flat plate theory as well as with one obtained from the time-marching steady transonic flow analysis of Reference 3. These quasi-static predictions were accomplished by maintaining the inlet flow vector and rotating the airfoil cascade. It should be noted that this quasi-static flat plate prediction is the zero frequency limit of the current state-of-the-art supersonic unstalled aerodynamic flutter analyses.

The quasi-static unsteady pressure coefficient data-prediction correlations on the suction surface are excellent, as seen in Figure 8. The discrepancies between the two predictions in the vicinity of the leading and trailing edges is attributed to the fact that the time-marching transonic analysis recognizes, to some extent, that the airfoils have a profile in these regions, whereas inviscid flat plate theory does not.

The quasi-static unsteady pressure coefficient data on the airfoil pressure surface correlates with the two predictions, as indicated in Figure 9. However, these correlations are not as good as those previously presented for the suction surface. The 50.64 percent chord data point is under the direct influence of the previously noted shocks which impinge on the airfoil pressure surface near mid-chord. Also, this pressure surface data is offset in level as compared to the quasi-static inviscid flat plate cascade prediction. However, the prediction overall trends as well as the magnitude of the increase in the value of the unsteady pressure coefficient across the mid-chord position shocks agree well with the quasi-static data. The time-marching steady flow analysis predicts a continuous, relatively smooth, static pressure distribution on the pressure surface at this level of loading, Figure 6. This results in the continuous, smooth, quasi-static unsteady pressure coefficient prediction on the airfoil pressure surface seen in Figure 9. Hence, the quasi-static prediction based on the transonic analysis does not correlate as well with the data as the one based on inviscid supersonic flat plate theory.

Upon completion of the quasi-static experiment, the airfoil cascade was harmonically oscillated in a torsional mode at a reduced frequency ($k = \omega b/U_\infty$) equal to 0.14 for specified

interblade phase angle values. At selected points the cascade static pressure ratio was increased from the nominal 1.05:1 to 1.30:1. Fundamental time-dependent aerodynamic data were then obtained, analyzed, and correlated with the predictions from the current state-of-the-art cascade analysis of Reference 4. This analysis assumes small perturbations which are generated by oscillating zero thickness flat plate cascaded airfoils in a uniform inviscid steady flowfield. Predictions were obtained for a variable blade-to-blade amplitude of oscillation, accomplished through input of the measured amplitudes into the analysis. The chordwise distribution of the complex data and the corresponding prediction is presented in the form of an aerodynamic phase lag as referenced to the motion of the instrumented airfoil, and the unsteady pressure coefficient, $C_p$, defined in Equation 1.

Figures 10 through 21 present the time-variant chordwise suction surface data and correlation with the variable amplitude flat plate cascade prediction for interblade phase angle values between - 32.3° and 193.8° and for two values of cascade static pressure ratio. It should be noted that the front portion of the suction surface is relatively flat, with a small precompression region located near the leading edge.

The aerodynamic phase lag data is seen to be in excellent agreement with the flat plate cascade prediction over the flat front portion of this suction surface. Over the rear half of this surface where the surface camber becomes significant, the data is seen to deviate from the flat plate prediction. For interblade phase angles near 45°, Figures 12 through 15, it is seen that the suction surface camber results in a decrease in the aerodynamic phase lag as compared to the flat plate prediction. For the other interblade phase angles investigated, the effect of the surface camber is to increase the phase lag as compared to the flat plate prediction. The absolute magnitude of the camber effect on the aerodynamic phase lag data is seen to be approximately equal for all of the cases. It is interesting to note that in this experiment, the cases for interblade phase angles near 45° were much more difficult to physically set up, i.e., it was much more difficult to achieve a constant interblade phase angle in the vicinity of 45°.

The effect of increased aerodynamic loading on the aerodynamic phase lag is demonstrated in Figures 14, 18, and 20. As seen, increased cascade static pressure ratio generally results in an increased phase lag over the cambered portion of the suction surface.

The chordwise trend of the suction surface unsteady pressure coefficient data is to decrease in the direction of the trailing edge. The data is increased significantly in value over the prediction for the front of the surface, decreasing in value and generally approaching the flat plate prediction near the trailing edge. This is an interesting contrast to the previously discussed phase lag data on this surface, in that the phase lag data correlated well with the flat plate prediction over the front portion of this surface. A similar trend has been previously noted in an experimental study of this instrumented blade as an isolated airfoil. It was speculated therein that this overall trend was caused by the leading edge region including the small precompression zone. Also, Figures 14, 18 and 20 demonstrate that an increased cascade static pressure ratio generally results in an increased unsteady pressure coefficient value over the rear of this surface.

Figures 22 through 33 present the time-variant chordwise pressure surface data together with the predictions obtained from the variable amplitude flat plate cascade prediction. The time-variant phenomena occurring on this surface are extremely complex as a cambered airfoil surface with two impinging shock waves are involved, depicted schematically in Figure 5.

Generally the aerodynamic phase lag data exhibits some correlation with the flat plate cascade prediction over the front portion of the pressure surface. The exception to this is the phase lag data for the cases with an interblade phase angle near 45°, Figures 24 through 27. For these cases, the leading edge phase lag data point, 14 percent chord, is noticably decreased in value as compared to the second chordwise data point, 34.5 percent chord, as well as the flat plate prediction. On the suction surface, a discrepancy was noted in the trend of the phase lag data over the cambered back portion of this surface for these same interblade phase angle cases. The pressure surface phase lag trend discrepancy is observed over the cambered front portion of this surface. Thus, this effect may be related to the influence of camber.

For the case of approximately 0° interblade phase angle, Figure 23, the aerodynamic phase lag data at the rearward chordwise data points downstream of the two shock wave impingement locations, are in relatively good agreement with the flat plate prediction. For all of the other interblade phase angle cases, Figures 22 and 28 through 33, the value of the aerodynamic phase lag approaches 360° in this trailing edge region. This may be attributable to the physical phenomena not modeled in the state-of-the-art flat plate cascade analysis. For example,

the analysis does not predict the pressure surface impingement of the shock wave originating at the trailing edge of the adjacent airfoil. Also, the steady flow field is modeled as a uniform flow with small unsteady perturbations superimposed. The nonlinearities of the flow field including airfoil camber, shock waves, their reflections and motion, are not modeled. That this may be significant is reflected in the fact that the 0° interblade phase angle case correlates well with the prediction over the back portion of the pressure surface whereas the other interblade phase cases do not. This 0° interblade phase angle case is special in that the shock systems do not interact with one another. For the other interblade phase angles investigated, this was not generally the case.

Overall, the unsteady pressure coefficient data on the pressure surface shows a relatively large decrease in value between the leading edge and the second chordwise data points, 14.0 percent and 34.5 percent chord, with this second data point demonstrating reasonable agreement with the flat plate prediction. The 65 percent chord data point is located in the immediate vicinity of the impinging trailing edge shock wave, hence the scatter exhibited by the data at this chordwise location between the various interblade phase angle cases. Over the approximate aft 40 percent of

the pressure surface, behind the trailing edge shock intersection, the unsteady pressure coefficient data is in reasonable agreement with the flat plate cascade prediction.

The effect of increased aerodynamic loading on the pressure surface unsteady data is demonstrated in Figures 26, 30, and 32. As indicated, increased cascade static pressure ratio generally results in an increased aerodynamic phase lag on the pressure surface, analogous to the suction surface results previously discussed.

## SUMMARY AND CONCLUSIONS

The unsteady cascade experiment directed at providing fundamental aerodynamic data necessary for the verification or the direction of refinements in the basic analytical model of unstalled supersonic torsional flutter in fans and compressors has been presented. This was accomplished by investigating an instrumented MCA airfoil cascade which modeled the tip section of an advanced design rotor blade. The steady airfoil surface aerodynamic performance was measured at two levels of aerodynamic loading and demonstrated very good correlation with the corresponding predictions obtained from a time-marching, steady, transonic flow analysis. A

quasi-static experiment was then conducted at a 0° interblade phase angle value. The resulting quasi-static unsteady pressure coefficient data was correlated with appropriate predictions from inviscid supersonic flat plate cascade theory as well as one obtained from the time-marching transonic analysis. The quasi-static unsteady pressure coefficient data exhibited excellent correlation with both predictions in the suction surface. On the pressure surface, however, the correlation was not as good, with somewhat better correlation of the data obtained with the flat plate prediction.

The dynamically instrumented MCA airfoil cascade was then harmonically oscillated in the torsional mode at an inlet Mach number of 1.55 over a range of interblade phase angle values for two cascade static pressure ratios. The fundamental unsteady MCA cascade aerodynamic obtained were then correlated with predictions from a state-of-the-art unsteady cascade variable blade-to-blade amplitude of oscillation analysis. The chordwise aerodynamic phase lag data is in excellent agreement with the flat plate cascade prediction over the flat front portion of the suction surface whereas the unsteady pressure coefficient data is increased in value over the prediction in this region. Over the rear cambered portion of this surface the phase lag data

deviates from the flat plate prediction whereas the unsteady pressure coefficient data approaches the prediction. The correlation of the flat plate prediction with the unsteady data on the cambered pressure surface is extremely complex. This is a result of the surface camber and the impingement of two shock waves on this surface. Generally, the phase lag data exhibits some correlation with the prediction over the front portion of the pressure surface. The unsteady pressure coefficient data exhibits a large decrease in the leading edge region of this surface, approaching the predicted value. Over the aft portion of this surface where the impinging shock waves are significant, the phase lag data correlates with the prediction for the case where the two shock systems do not interact. When these two systems do interact, the flat plate prediction and the phase lag data do not correlate.

It should be noted that many of the trends of this MCA unsteady data have been previously noted. The increased values of the unsteady pressure coefficient in the leading regions were found in an isolated airfoil investigation using this same airfoil. Also, Reference 6 presents the results of an unsteady cascade experiment wherein the airfoils were fixed but the upstream wedge was oscillated to generate an unsteady

inlet flow field. The same MCA profile blading was used, although not the same instrumented airfoil. Therein are presented aerodynamic phase lag and unsteady pressure magnitude data in the pressure and suction surfaces which show a remarkable similarity in trend to the data presented herein.

| | |
|---|---|
| CHORD | 2.50 INCH (6.35 CM) |
| SOLIDITY | 1.21 |
| MAXIMUM THICKNESS/CHORD | 0.03 |
| MAXIMUM THICKNESS LOCATION | 50% CHORD |
| SETTING ANGLE | 66.09° (1.15 RADIANS) |
| LEADING EDGE RADIUS/CHORD | 0.0015 |
| TORSIONAL AXIS LOCATION | 50% CHORD |

TABLE I. CASCADE PHYSICAL PARAMETERS

| SUCTION SURFACE | | PRESSURE SURFACE | |
|---|---|---|---|
| X/C* | Y/C* | X/C* | Y/C* |
| 0.00 | 0.86 | 0.00 | 0.71 |
| 5.21 | 0.98 | 6.29 | 0.04 |
| 11.53 | 0.96 | 12.59 | - 0.53 |
| 17.84 | 0.96 | 18.90 | - 1.00 |
| 24.14 | 0.97 | 25.21 | - 1.37 |
| 30.45 | 0.99 | 31.53 | - 1.64 |
| 36.75 | 1.02 | 37.85 | - 1.81 |
| 43.05 | 1.08 | 44.18 | - 1.88 |
| 49.35 | 1.12 | 50.51 | - 1.85 |
| 55.65 | 1.22 | 56.83 | - 1.72 |
| 61.95 | 1.31 | 63.15 | - 1.48 |
| 68.25 | 1.41 | 69.47 | - 1.15 |
| 74.55 | 1.53 | 75.78 | - 0.71 |
| 80.88 | 1.62 | 82.06 | - 0.25 |
| 87.21 | 1.58 | 88.36 | 0.16 |
| 93.53 | 1.38 | 94.66 | 0.50 |
| 99.85 | 1.02 | 99.86 | 0.88 |

*Expressed in percent.

TABLE II. MCA AIRFOIL PROFILE COORDINATES

| PRESSURE SURFACE | SUCTION SURFACE |
|---|---|
| 13.99 | 14.05 |
| 24.08 | 24.14 |
| 32.93 | 32.97 |
| 41.79 | 41.79 |
| 50.64 | 50.61 |
| 67.08 | 66.99 |
| 75.92 | 75.81 |
| 84.72 | 84.67 |

TABLE III. PERCENT CHORD LOCATIONS OF AIRFOIL SURFACE STATIC PRESSURE TAPS

| PRESSURE SURFACE | SUCTION SURFACE |
|---|---|
| 14.0 | 36.0 |
| 34.5 | 55.0 |
| 65.0 | 65.0 |
| 75.5 | 74.5 |
| 87.0 | 85.0 |

TABLE IV. PERCENT CHORD LOCATIONS OF AIRFOIL SURFACE DYNAMIC PRESSURE TRANSDUCERS

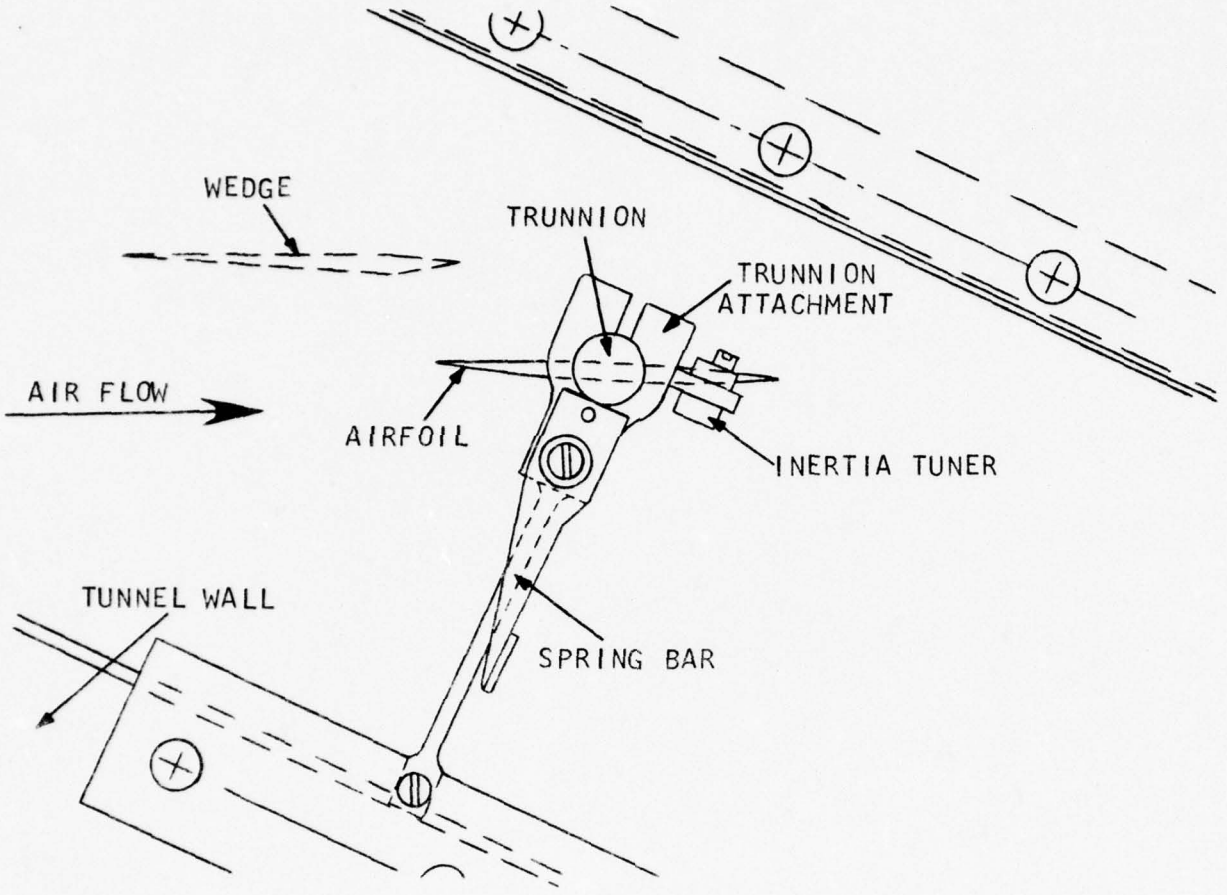


FIGURE 1. SCHEMATIC OF AIRFOIL-SPRING BAR MOUNTING ARRANGEMENT

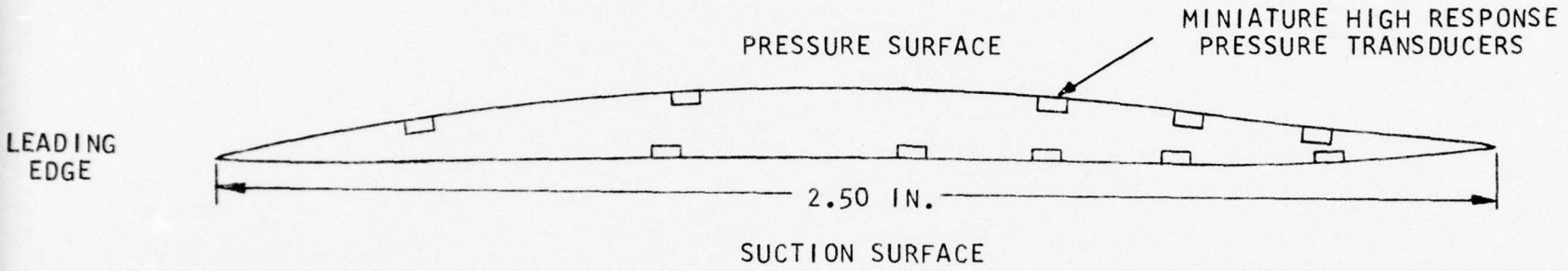


FIGURE 2. MCA AIRFOIL PROFILE

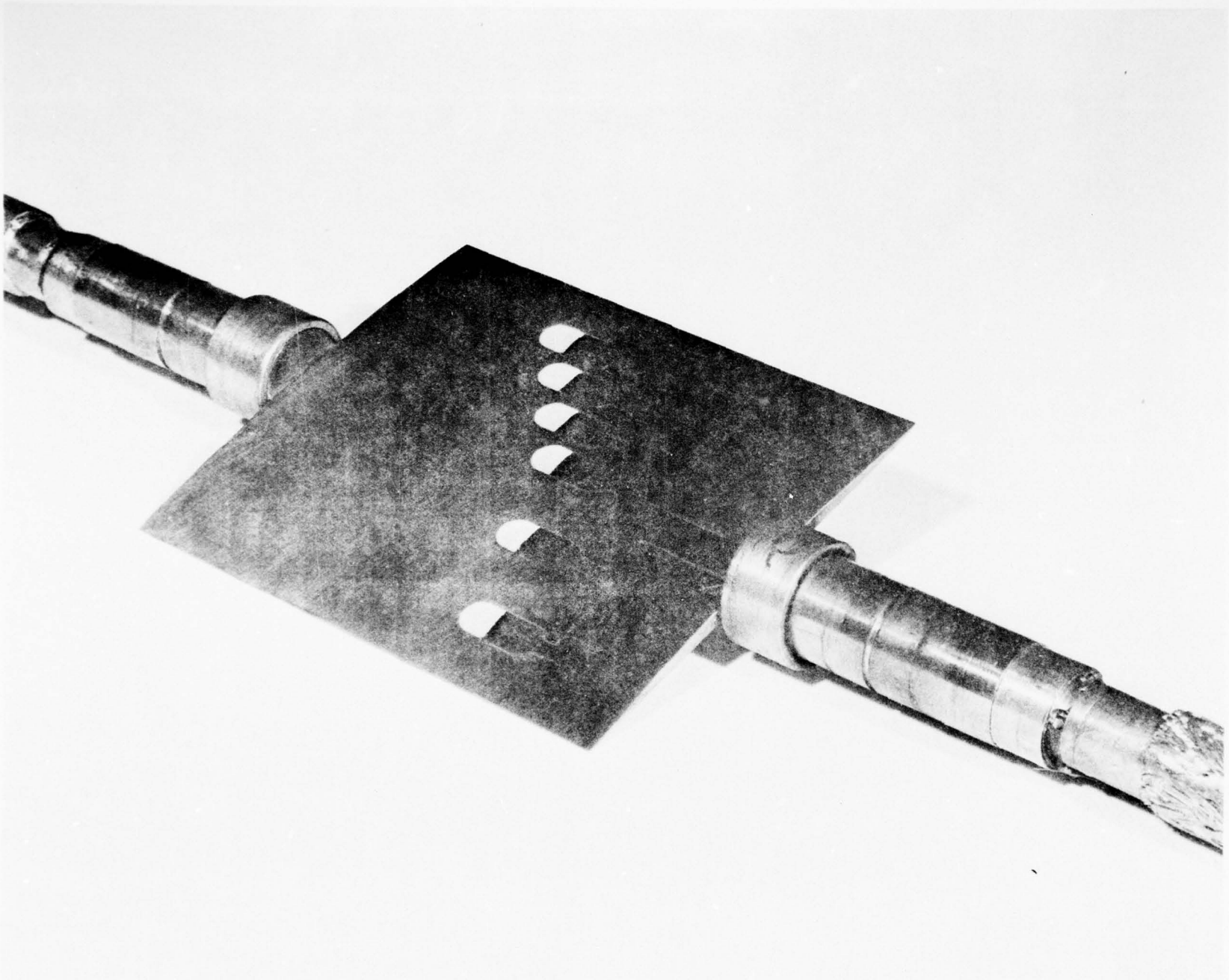

FIGURE 3. PRESSURE SURFACE OF INSTRUMENTED MCA AIRFOIL

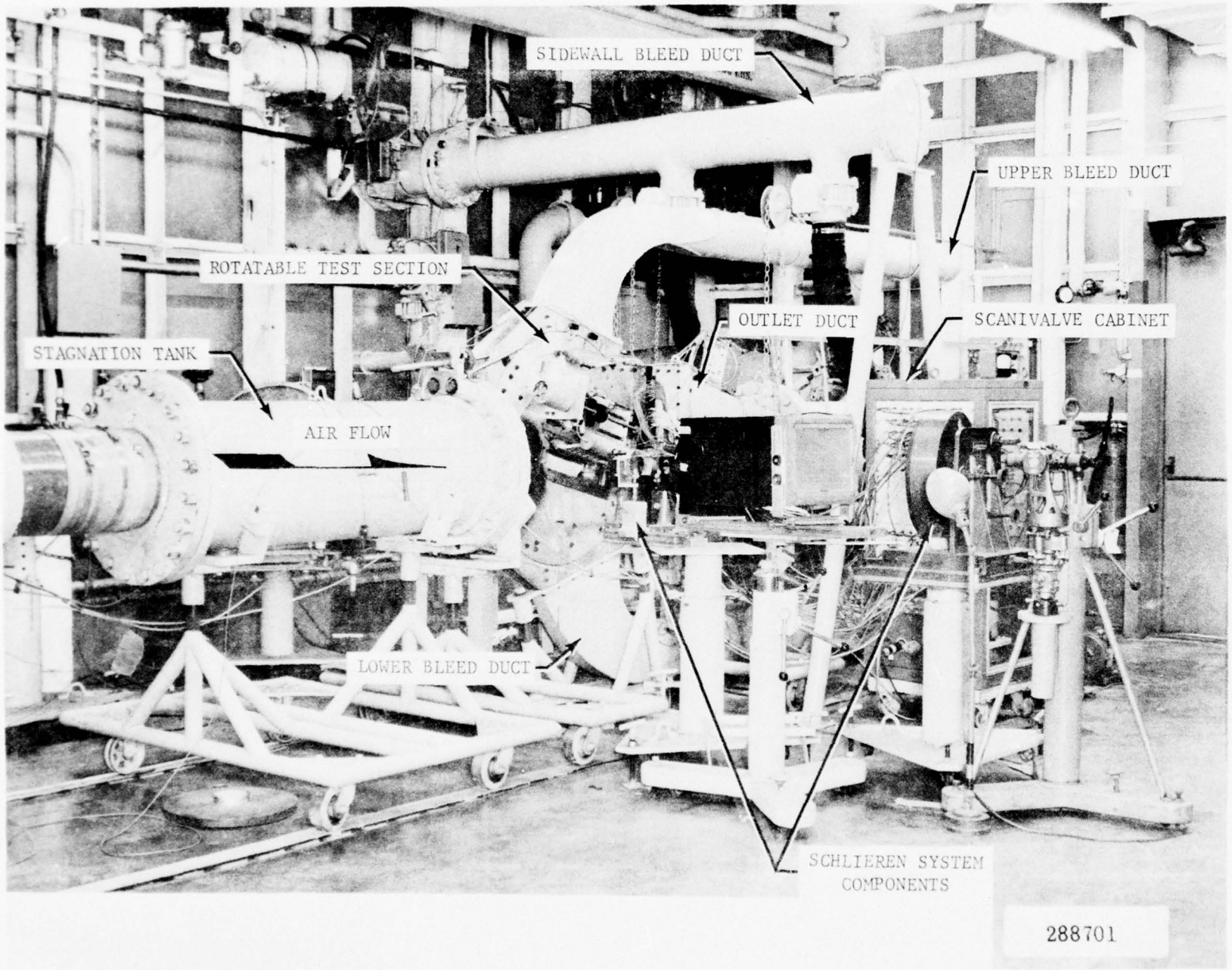


FIGURE 4. OVERALL VIEW OF RECTILINEAR CASCADE FACILITY

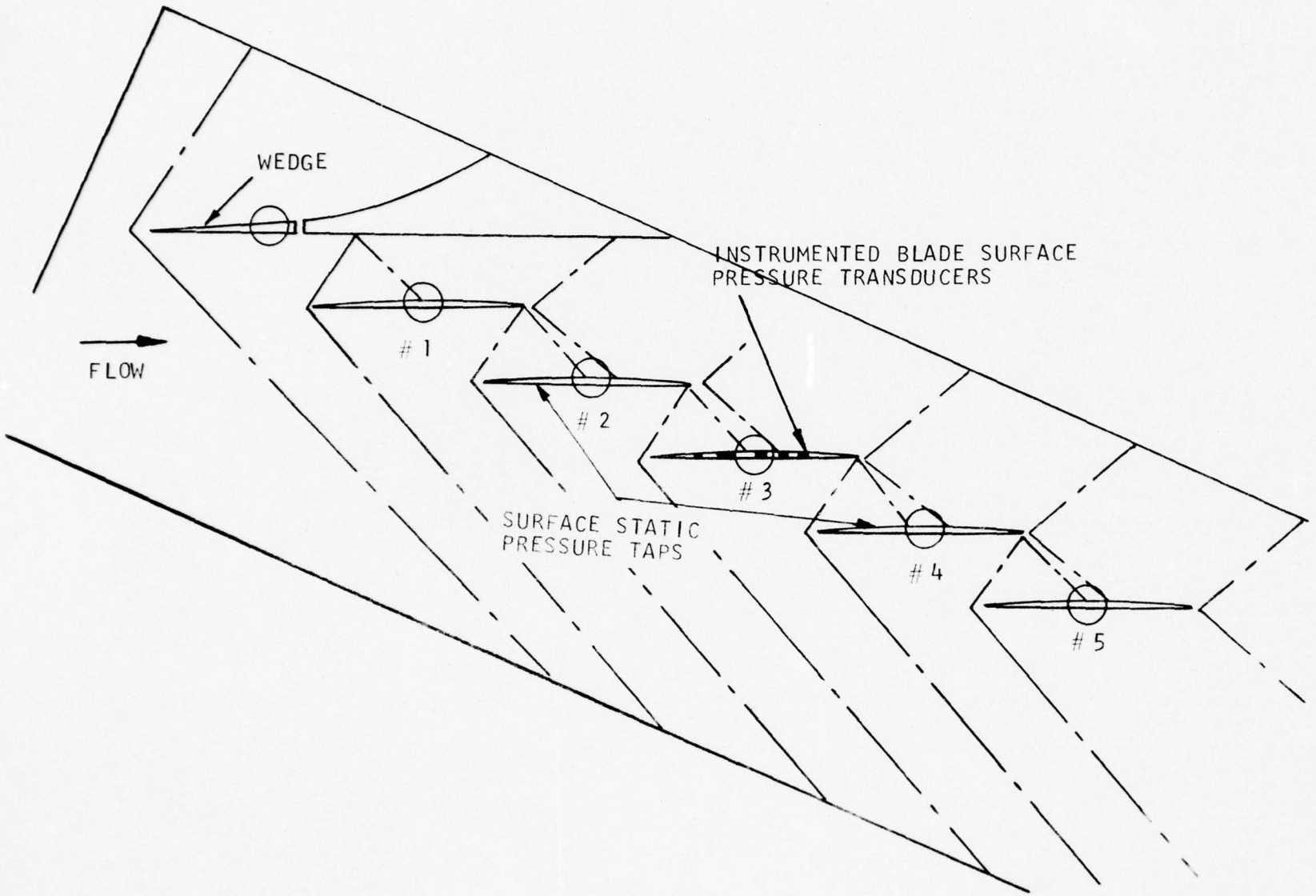


FIGURE 5. SCHEMATIC OF CASCADE FLOW FIELD

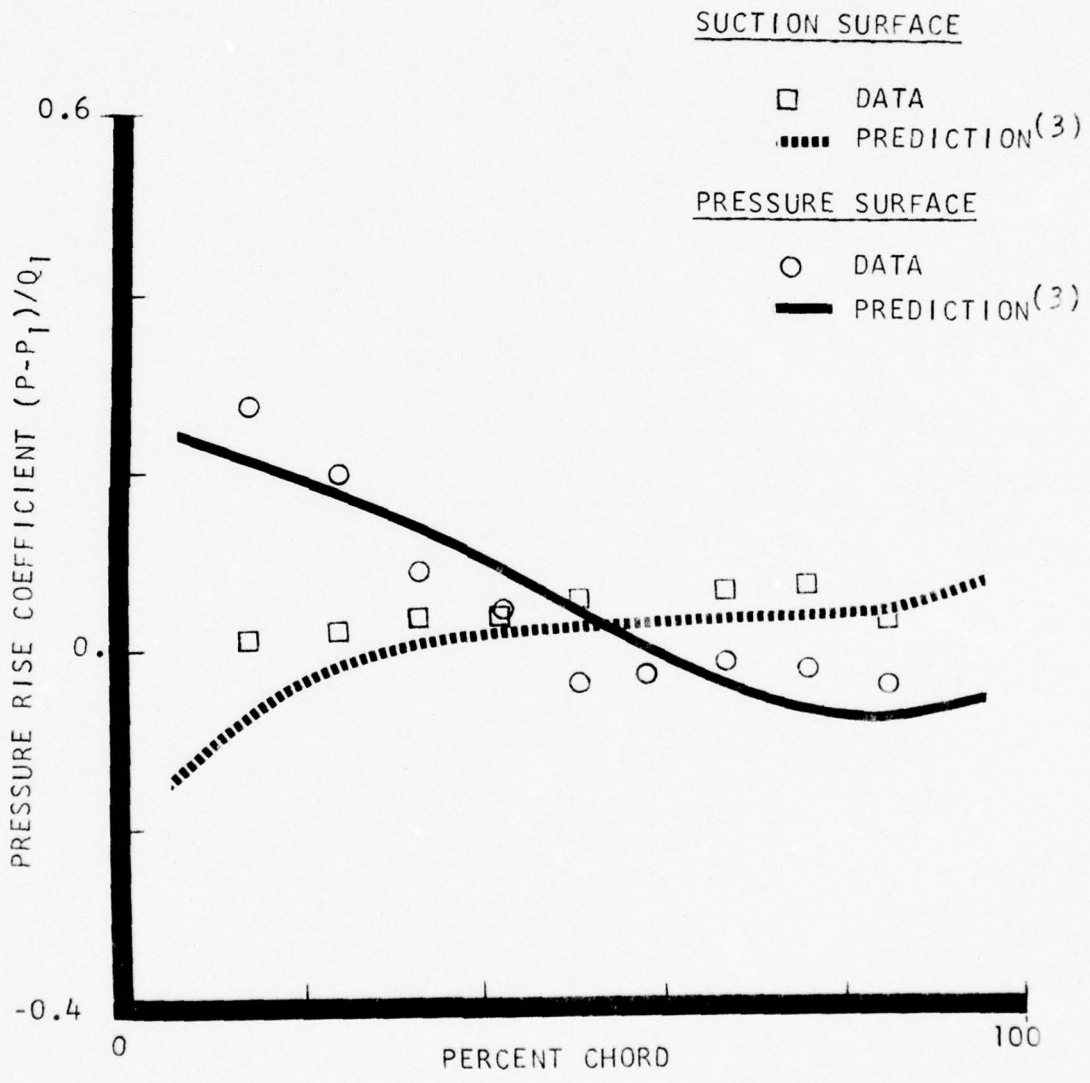


FIGURE 6. AIRFOIL SURFACE STEADY AERODYNAMIC PERFORMANCE FOR AN INLET MACH NUMBER OF 1.55 AND A CASCADE STATIC PRESSURE RATIO OF 1.05:1

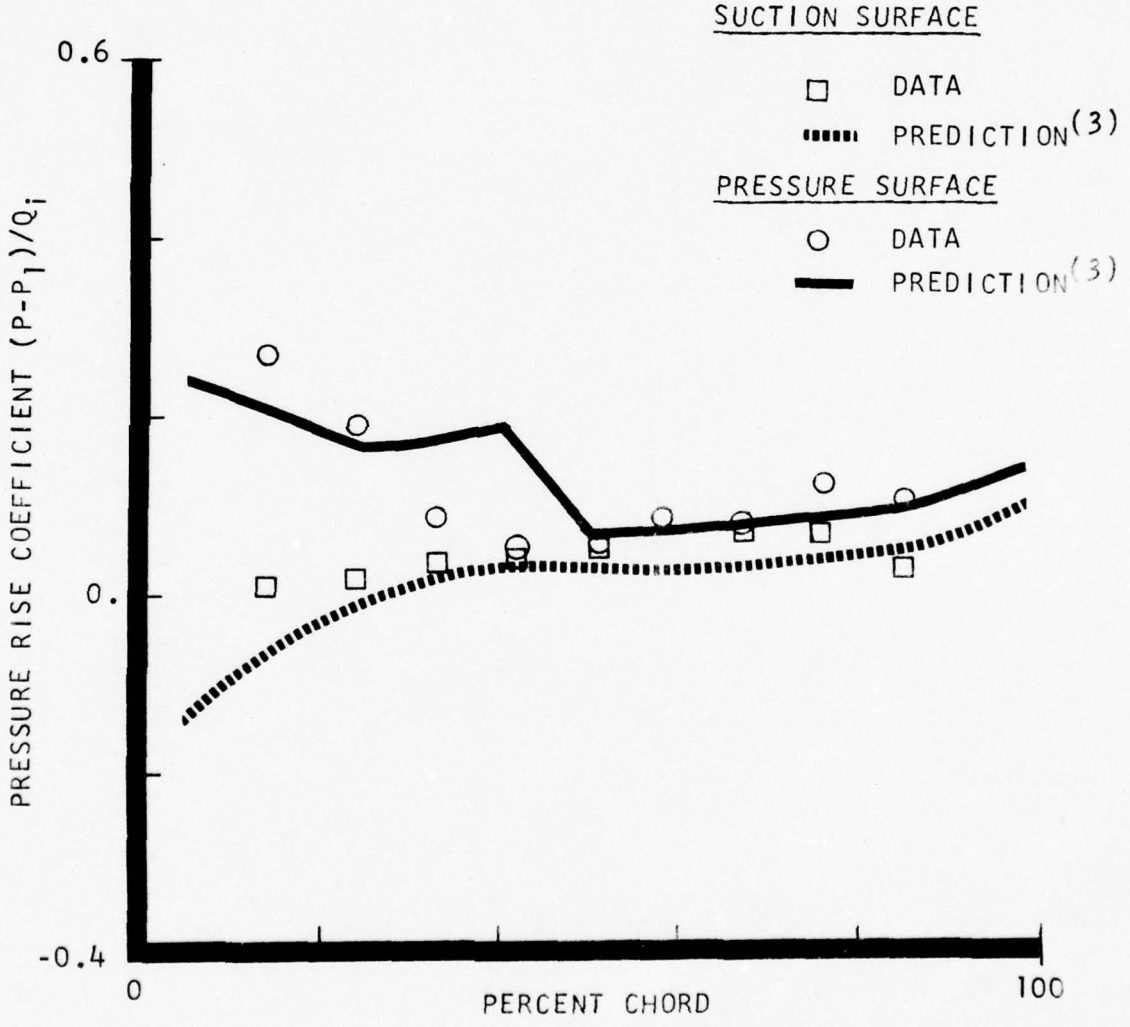


FIGURE 7. AIRFOIL SURFACE STEADY AERODYNAMIC PERFORMANCE FOR AN INLET MACH NUMBER OF 1.55 AND A CASCADE STATIC PRESSURE RATIO OF 1.30:1

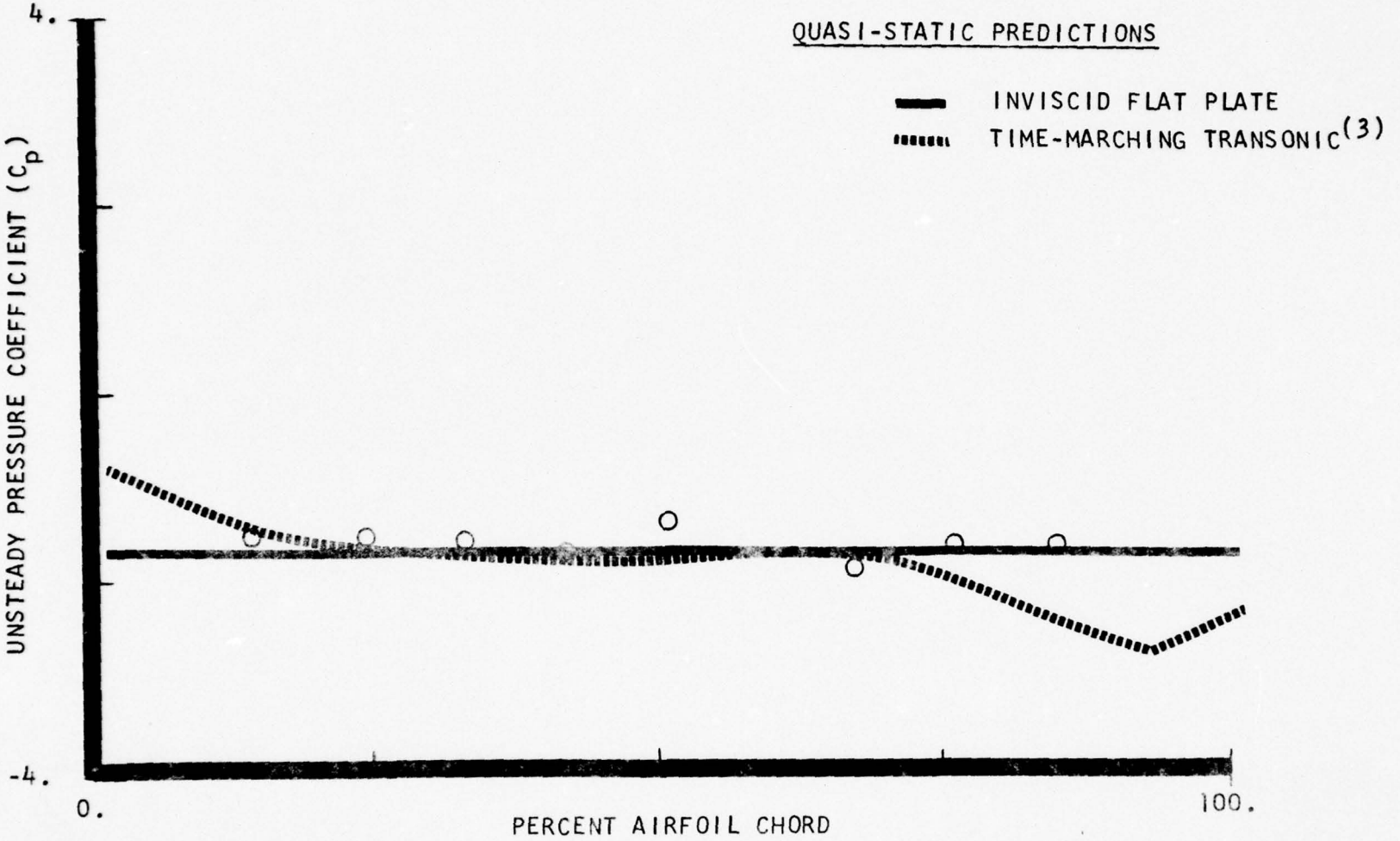


FIGURE 8. SUCTION SURFACE QUASI-STATIC UNSTEADY PRESSURE COEFFICIENT DATA AND PREDICTIONS FOR A 0° INTERBLADE PHASE ANGLE

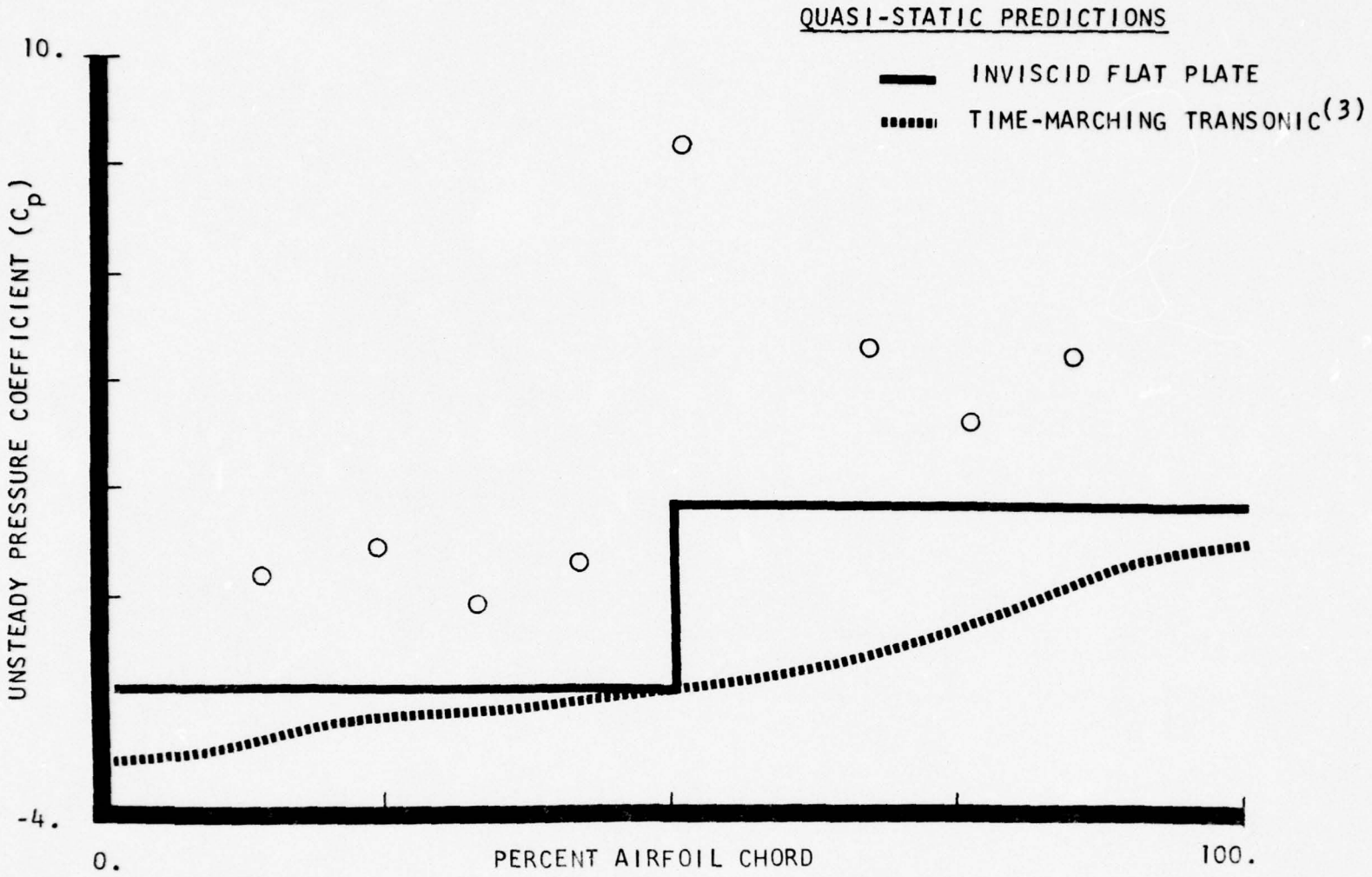


FIGURE 9. PRESSURE SURFACE QUASI-STATIC UNSTEADY PRESSURE COEFFICIENT DATA AND PREDICTIONS FOR A 0° INTERBLADE PHASE ANGLE

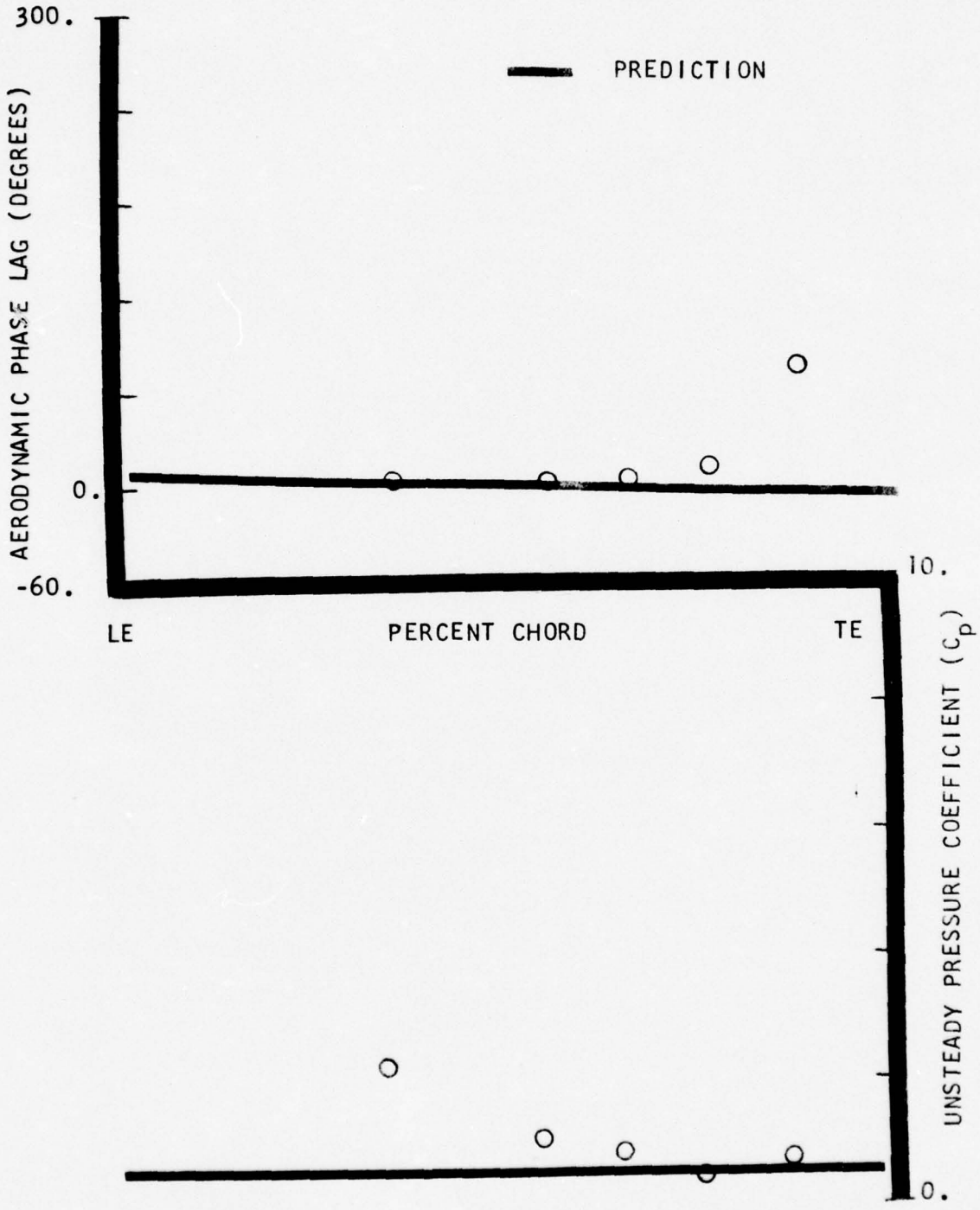


FIGURE 10. CHORDWISE DISTRIBUTION OF THE UNSTEADY CASCADE DATA AND CORRESPONDING FLAT PLATE PREDICTIONS ON THE AIRFOIL SUCTION SURFACE FOR A -32.3° INTERBLADE PHASE ANGLE AT A STATIC PRESSURE RATIO OF 1.05:1

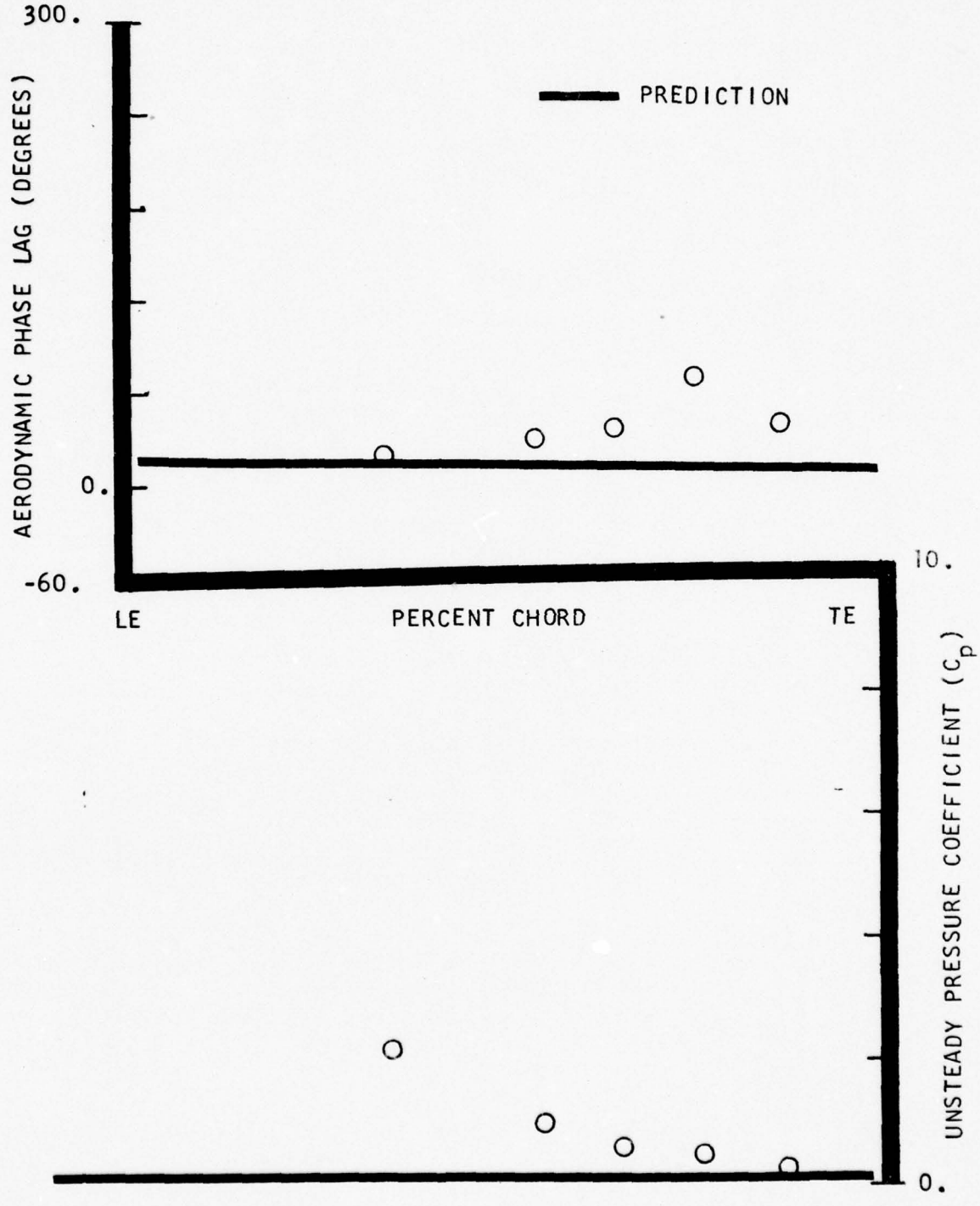


FIGURE 11. CHORDWISE DISTRIBUTION OF THE UNSTEADY CASCADE DATA AND CORRESPONDING FLAT PLATE PREDICTIONS ON THE AIRFOIL SUCTION SURFACE FOR A -4.4° INTERBLADE PHASE ANGLE AT A STATIC PRESSURE RATIO OF 1.05:1

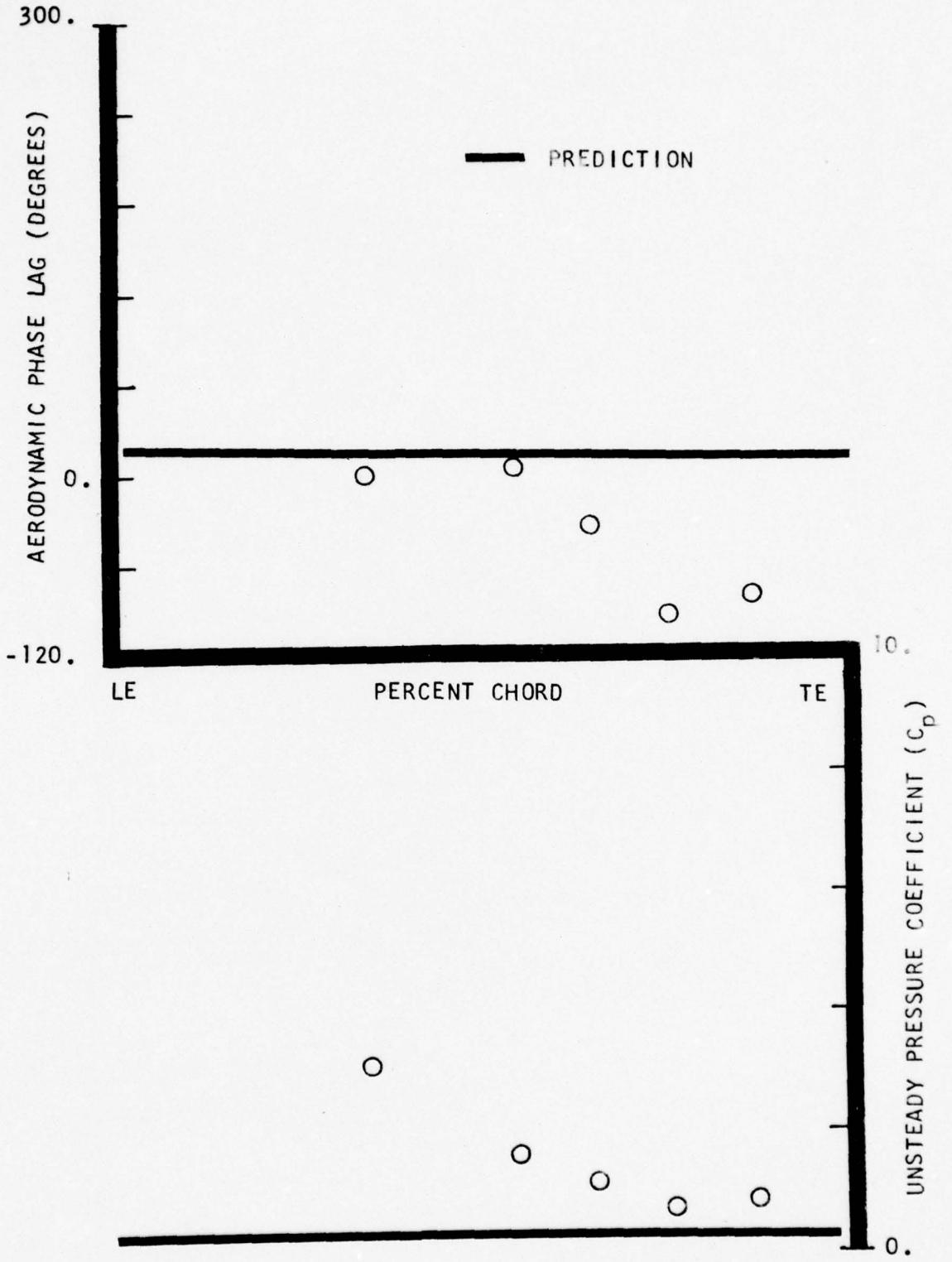


FIGURE 12. CHORDWISE DISTRIBUTION OF THE UNSTEADY CASCADE DATA AND CORRESPONDING FLAT PLATE PREDICTIONS ON THE AIRFOIL SUCTION SURFACE FOR A 46.6° INTERBLADE PHASE ANGLE AT A STATIC PRESSURE RATIO OF 1.05:1

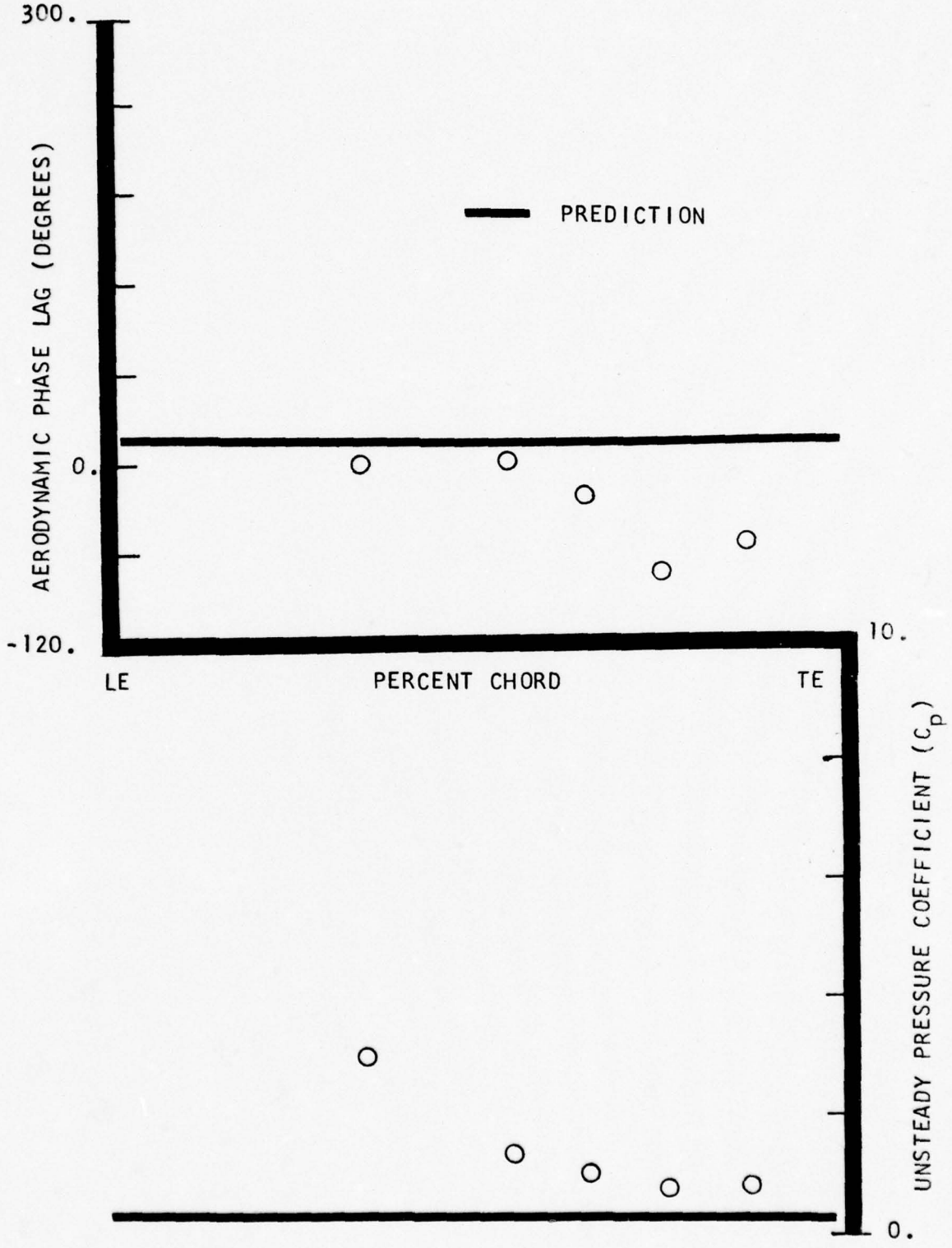


FIGURE 13. CHORDWISE DISTRIBUTION OF THE UNSTEADY CASCADE DATA AND CORRESPONDING FLAT PLATE PREDICTIONS ON THE AIRFOIL SUCTION SURFACE FOR A 58.2° INTERBLADE PHASE ANGLE AT A STATIC PRESSURE RATIO OF 1.05:1

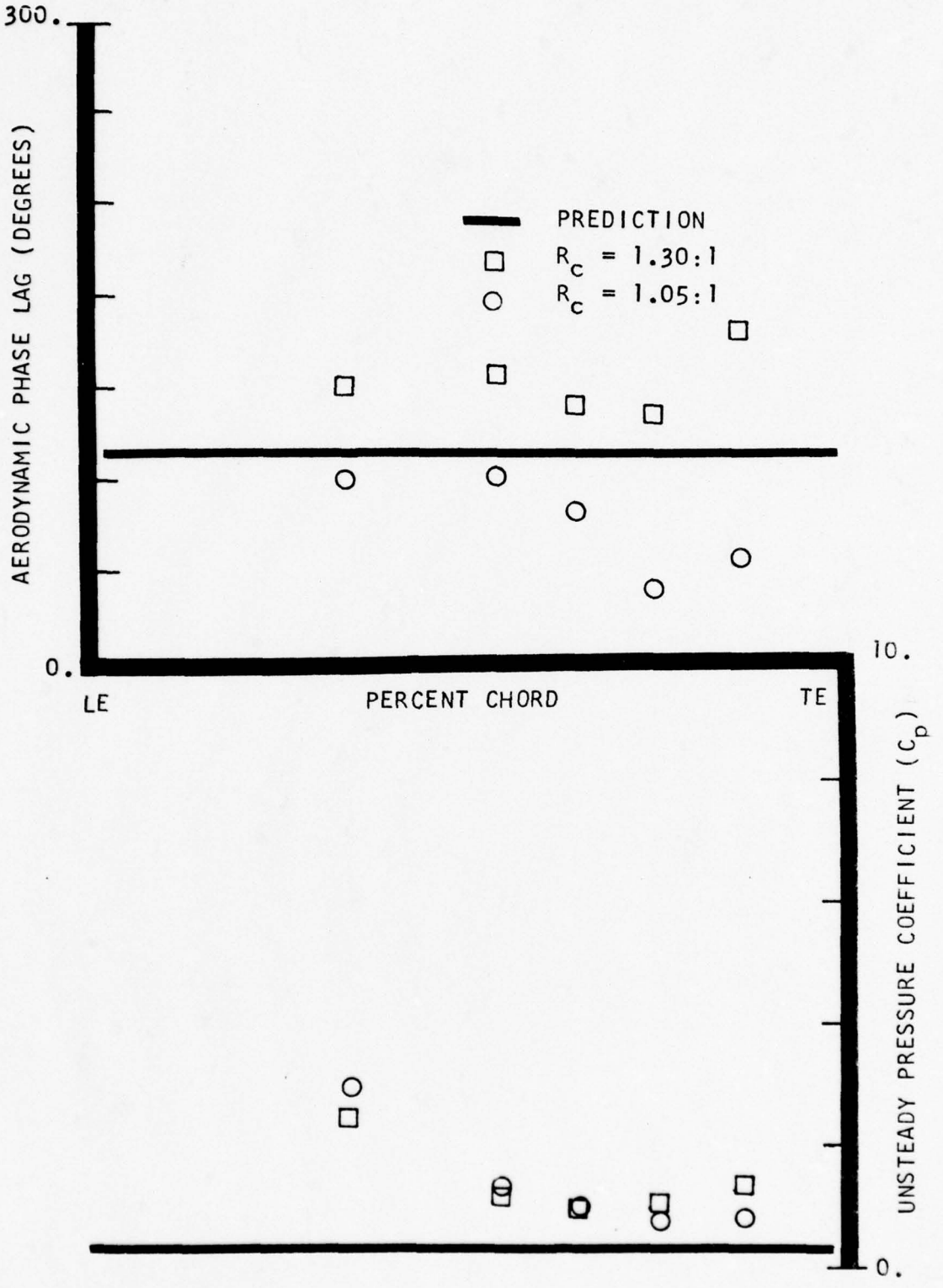


FIGURE 14. CHORDWISE DISTRIBUTION OF THE UNSTEADY CASCADE DATA AND CORRESPONDING FLAT PLATE PREDICTIONS ON THE AIRFOIL SUCTION SURFACE FOR 56.7° AND 58.2° INTERBLADE PHASE ANGLES AT THE STATIC PRESSURE RATIOS OF 1.30:1 AND 1.05:1, RESPECTIVELY

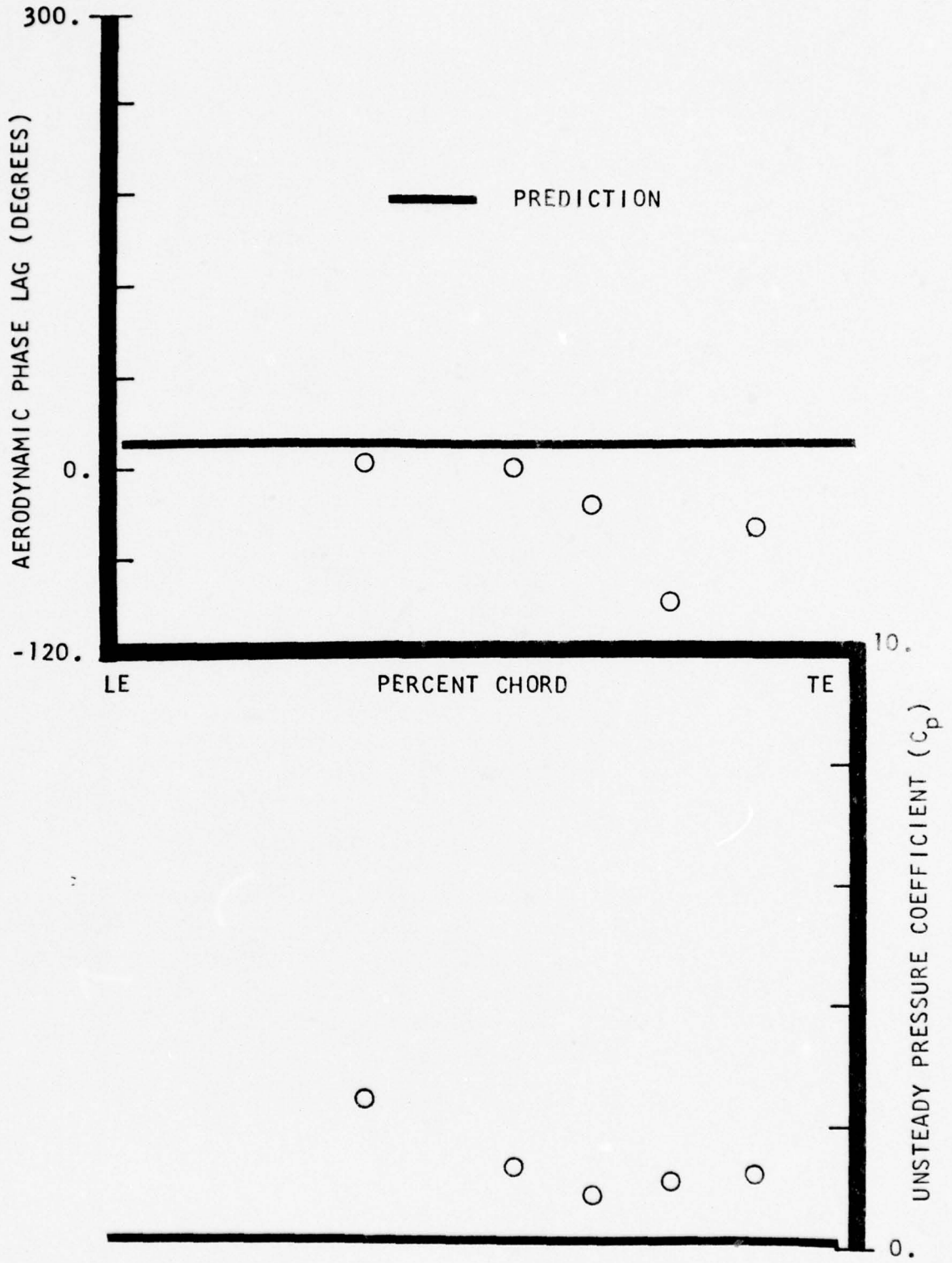


FIGURE 15. CHORDWISE DISTRIBUTION OF THE UNSTEADY CASCADE DATA AND CORRESPONDING FLAT PLATE PREDICTIONS ON THE AIRFOIL SUCTION SURFACE FOR A 70.2° INTERBLADE PHASE ANGLE AT A STATIC PRESSURE RATIO OF 1.05:1

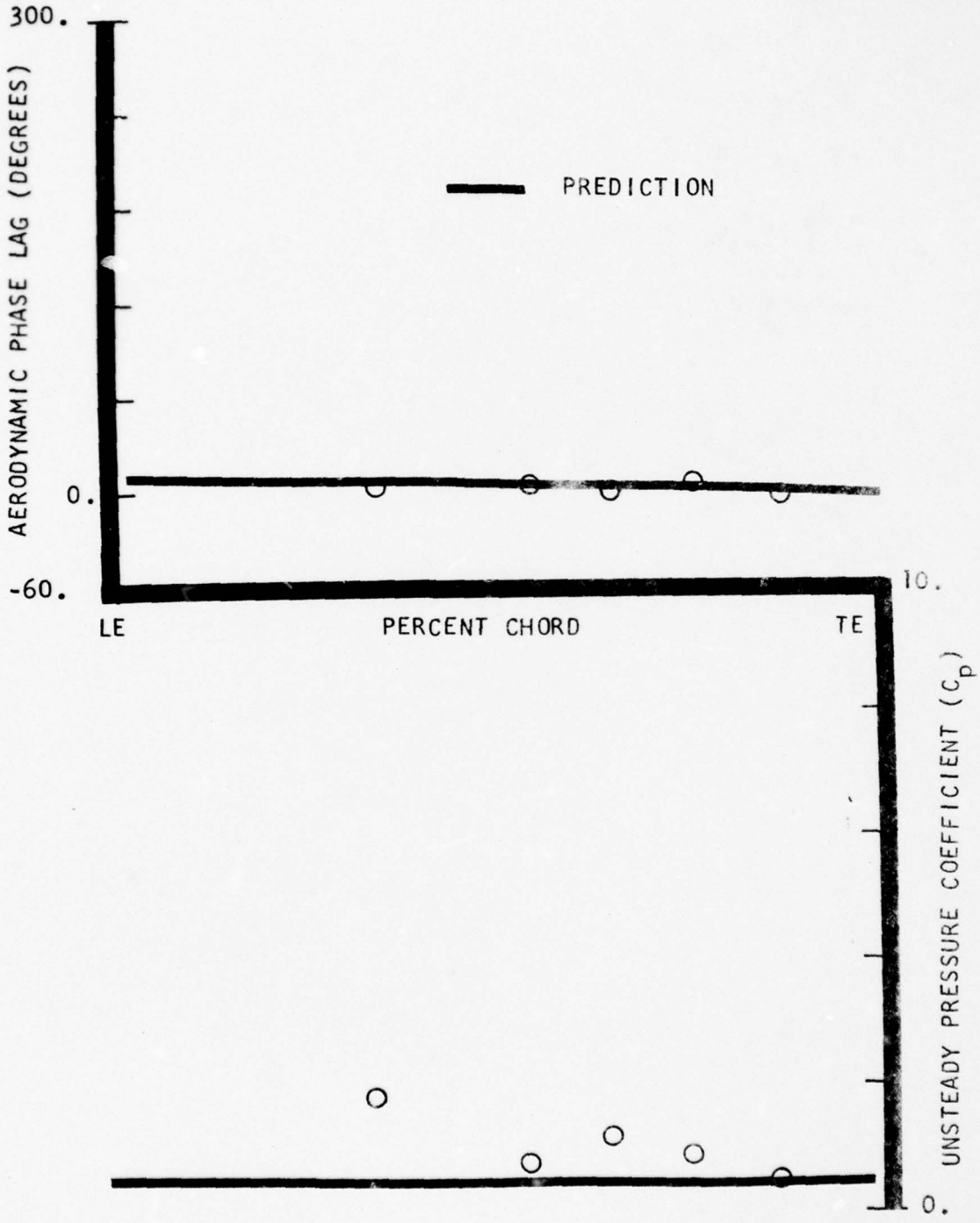


FIGURE 16. CHORDWISE DISTRIBUTION OF THE UNSTEADY CASCADE DATA AND CORRESPONDING FLAT PLATE PREDICTIONS ON THE AIRFOIL SUCTION SURFACE FOR A 130.6° INTERBLADE PHASE ANGLE AT A STATIC PRESSURE RATIO OF 1.05:1

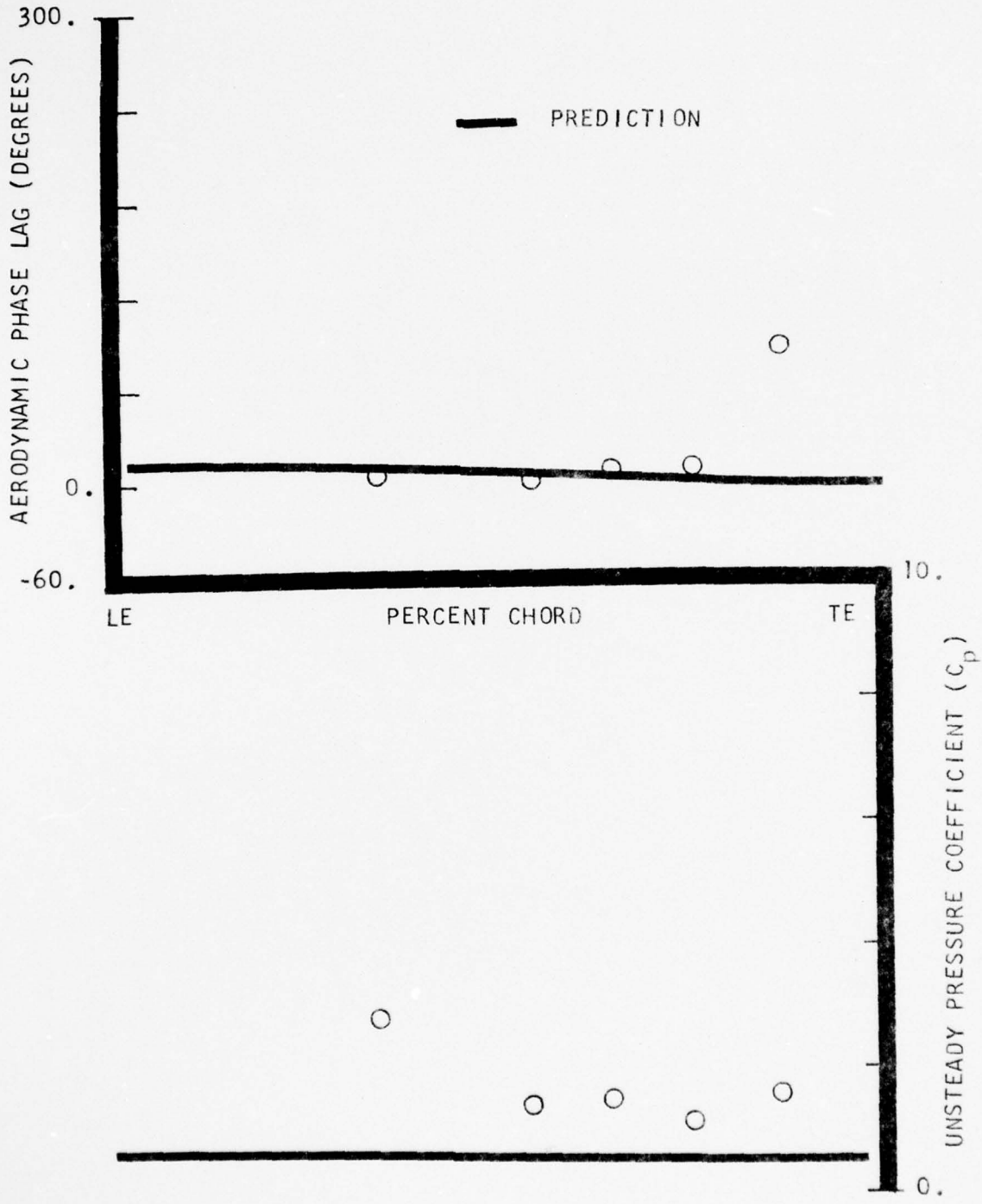


FIGURE 17. CHORDWISE DISTRIBUTION OF THE UNSTEADY CASCADE DATA AND CORRESPONDING FLAT PLATE PREDICTIONS ON THE AIRFOIL SUCTION SURFACE FOR A 162.1° INTERBLADE PHASE ANGLE AT A STATIC PRESSURE RATIO OF 1.05:1

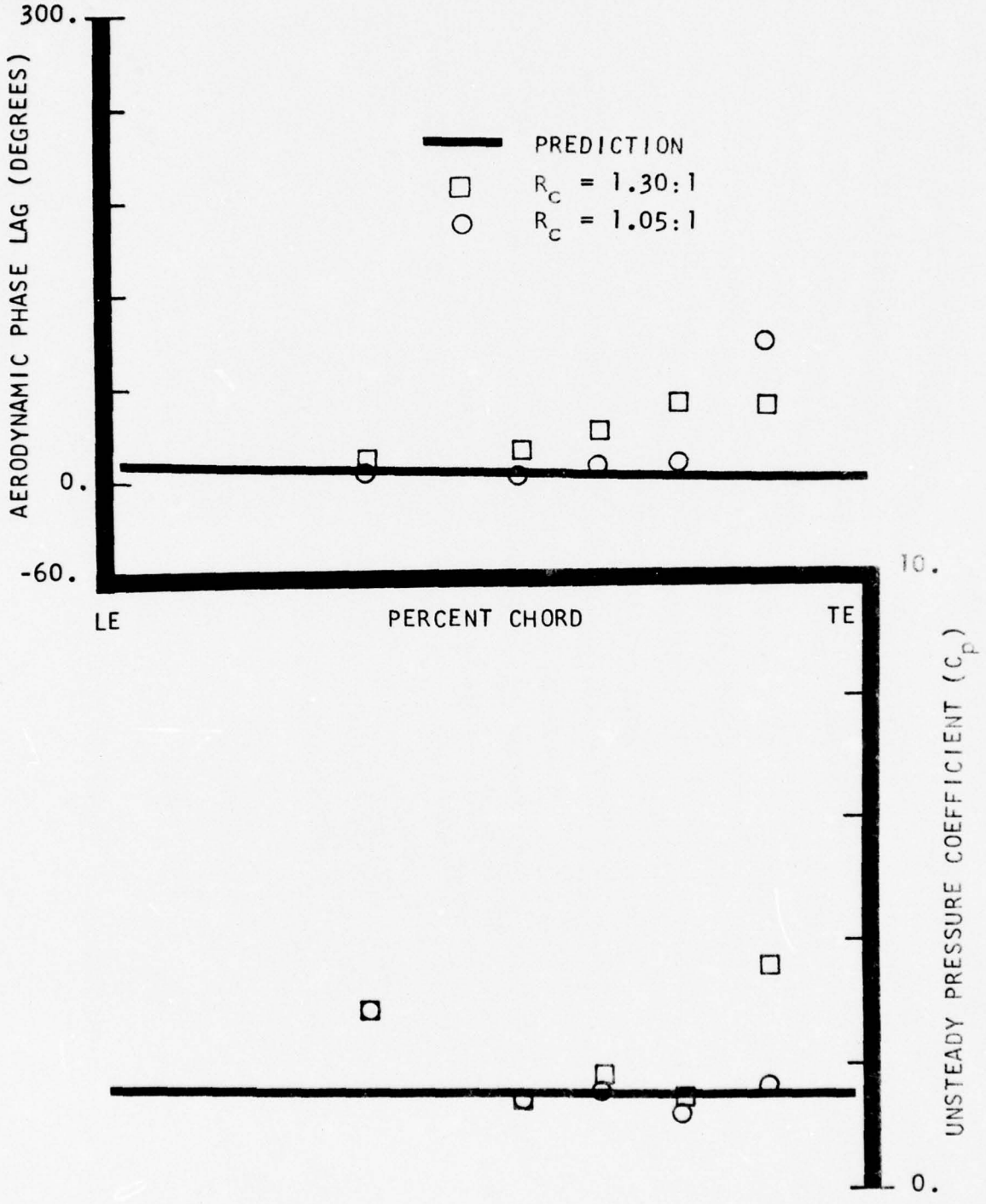


FIGURE 18. CHORDWISE DISTRIBUTION OF THE UNSTEADY CASCADE DATA AND CORRESPONDING FLAT PLATE PREDICTIONS ON THE AIRFOIL SUCTION SURFACE FOR 163.1° AND 162.1° INTERBLADE PHASE ANGLES AT STATIC PRESSURE RATIOS OF 1.30:1 AND 1.05:1, RESPECTIVELY

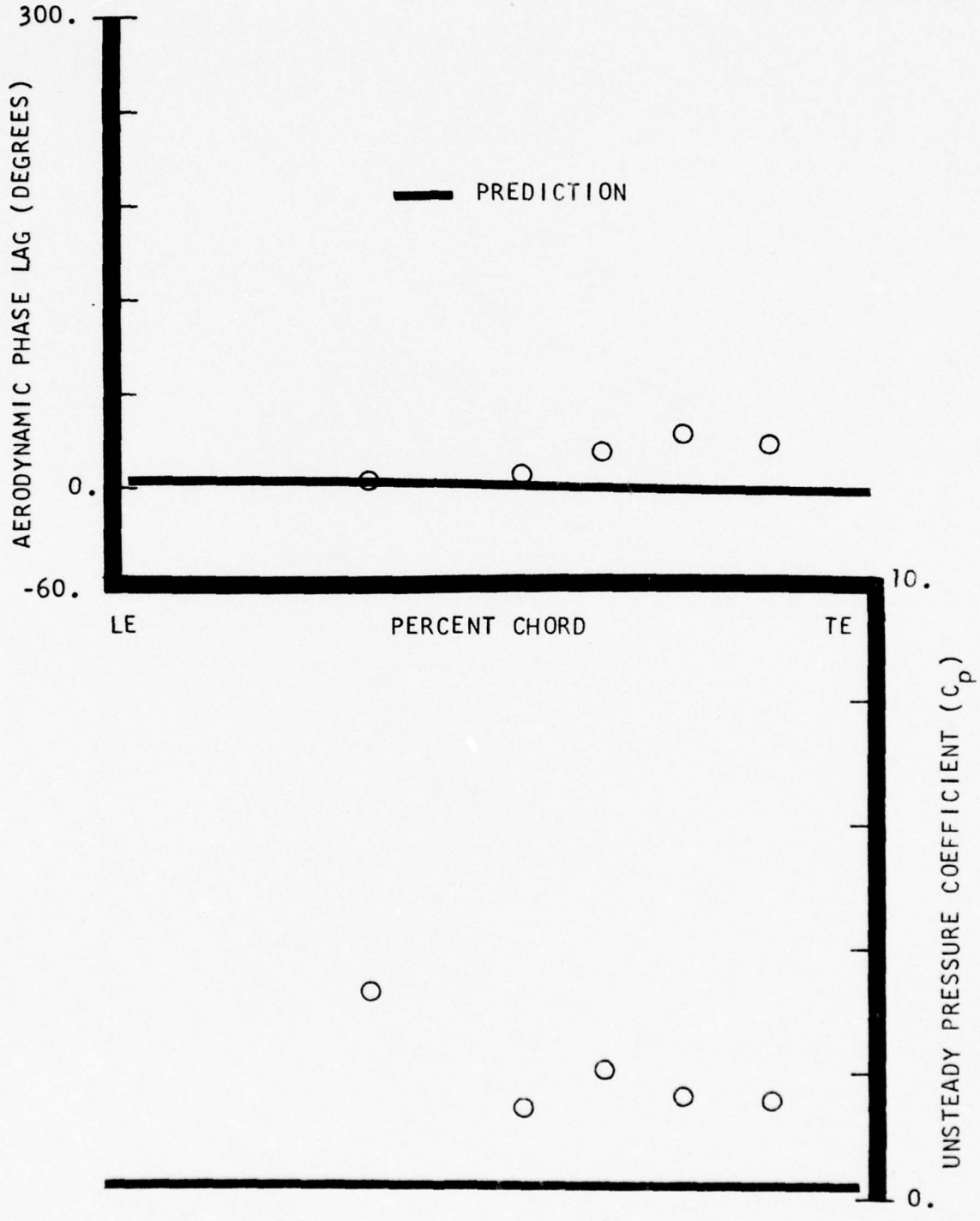


FIGURE 19. CHORDWISE DISTRIBUTION OF THE UNSTEADY CASCADE DATA AND CORRESPONDING FLAT PLATE PREDICTIONS ON THE AIRFOIL SUCTION SURFACE FOR A 170.2° INTERBLADE PHASE ANGLE AT A STATIC PRESSURE RATIO OF 1.05:1

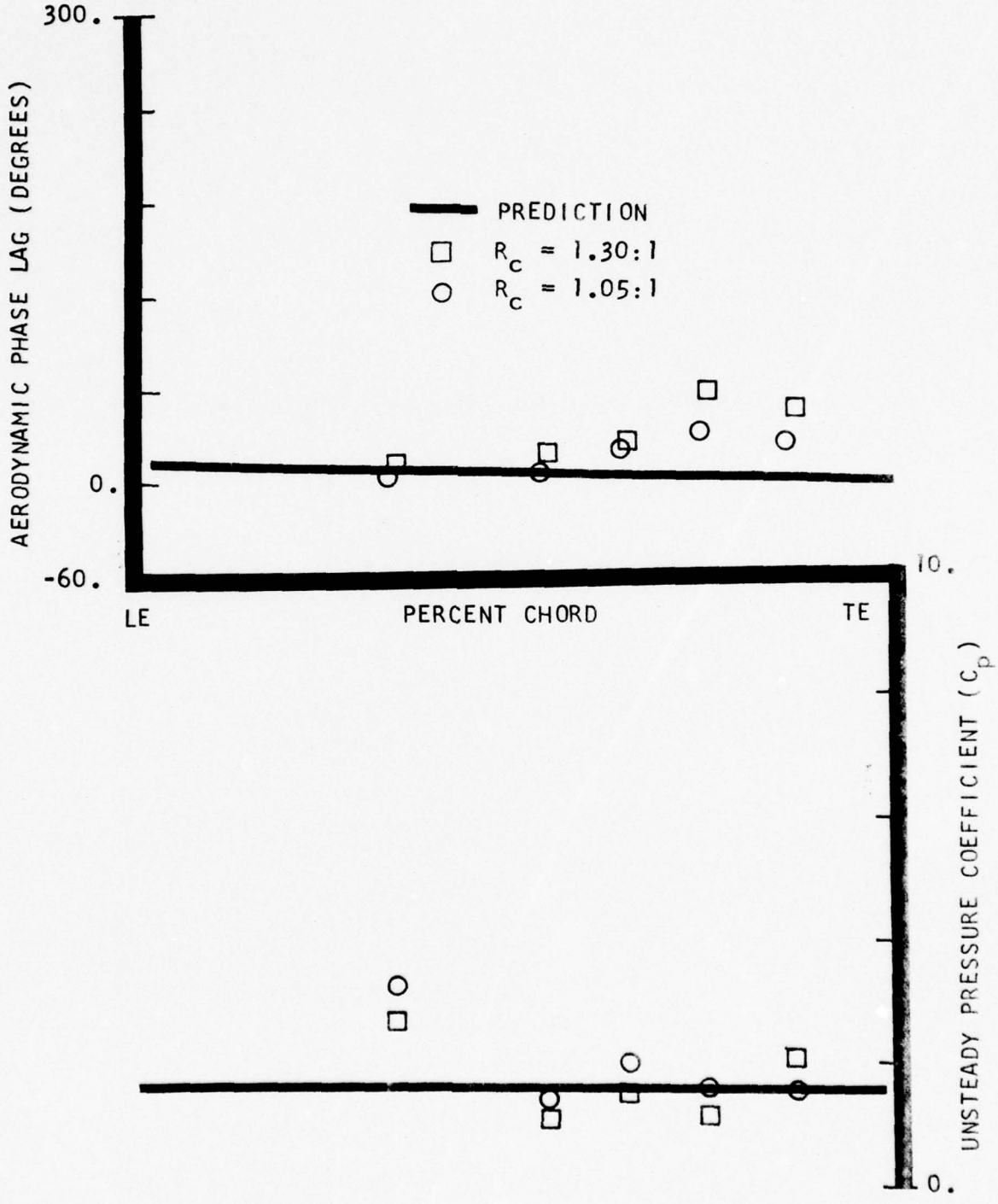


FIGURE 20. CHORDWISE DISTRIBUTION OF THE UNSTEADY CASCADE DATA AND CORRESPONDING FLAT PLATE PREDICTIONS ON THE AIRFOIL SUCTION SURFACE FOR 173.4° AND 170.2° INTERBLADE PHASE ANGLES AT STATIC PRESSURE RATIOS OF 1.30:1 AND 1.05:1, RESPECTIVELY

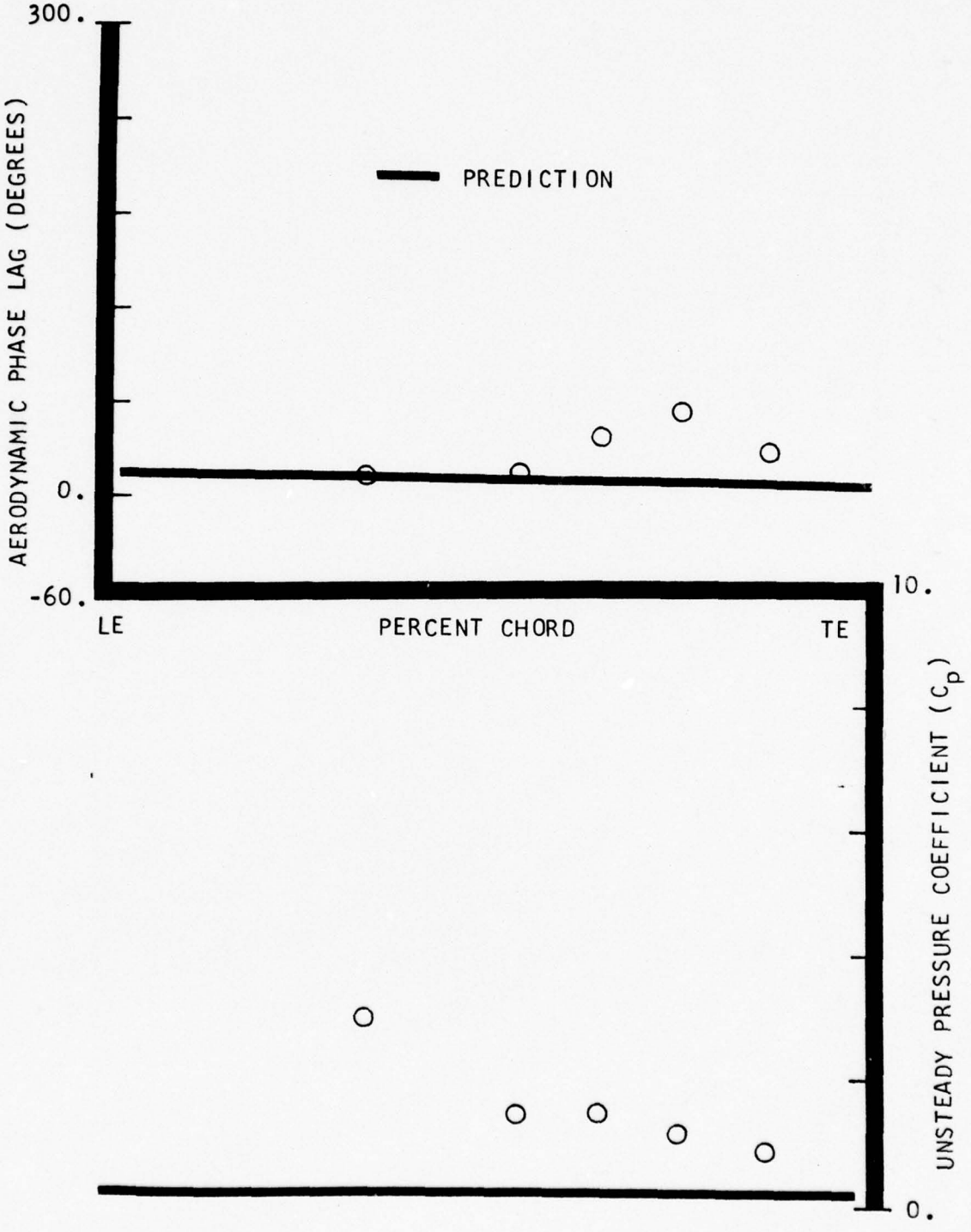


FIGURE 21. CHORDWISE DISTRIBUTION OF THE UNSTEADY CASCADE DATA AND CORRESPONDING FLAT PLATE PREDICTIONS ON THE AIRFOIL SUCTION SURFACE FOR A 193.8° INTERBLADE PHASE ANGLE AT A STATIC PRESSURE RATIO OF 1.05:1

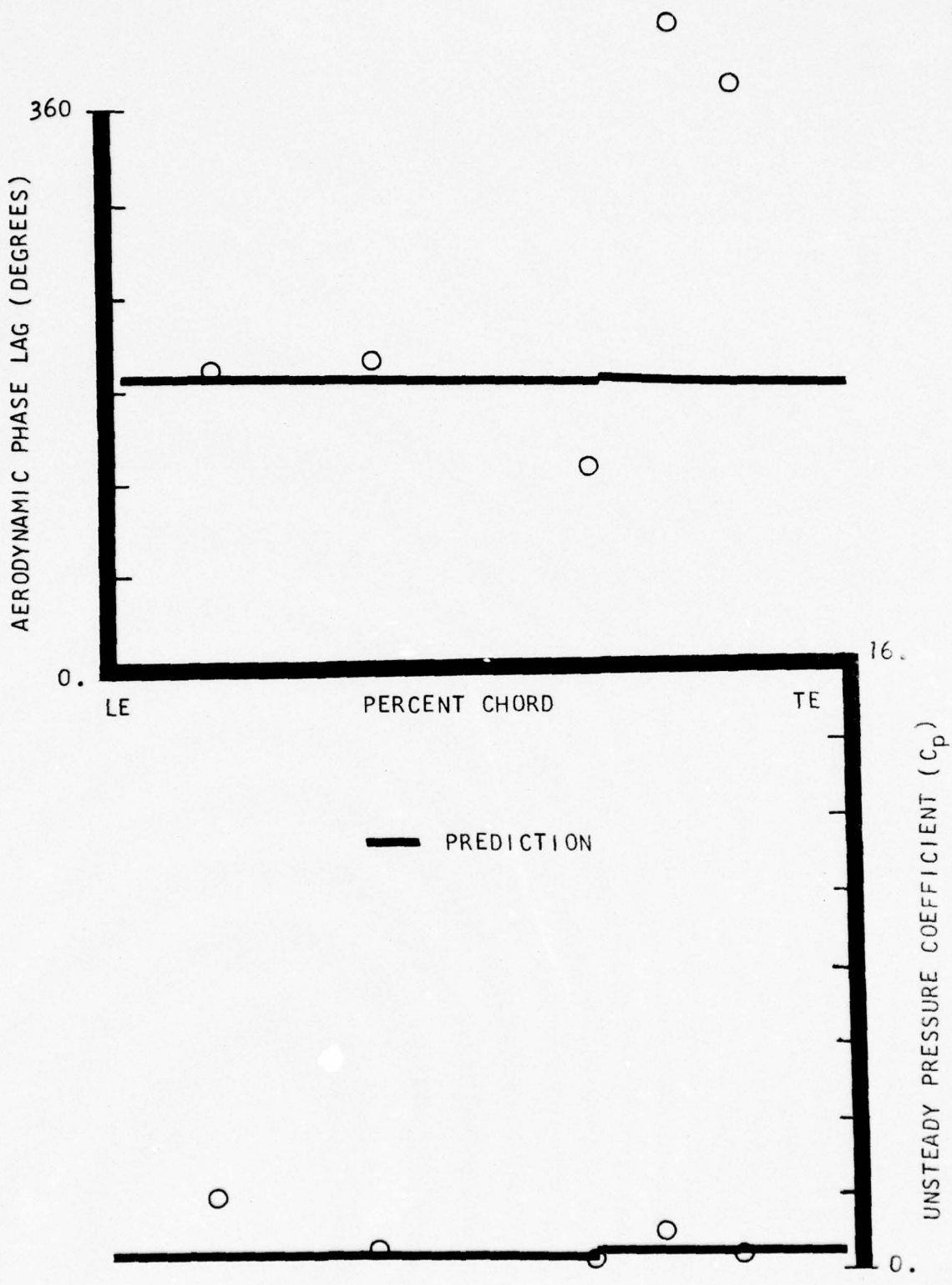


FIGURE 22. CHORDWISE DISTRIBUTION OF THE UNSTEADY CASCADE DATA AND CORRESPONDING FLAT PLATE PREDICTIONS ON THE AIRFOIL PRESSURE SURFACE FOR A -32.3° INTERBLADE PHASE ANGLE AT A STATIC PRESSURE RATIO OF 1.05:1

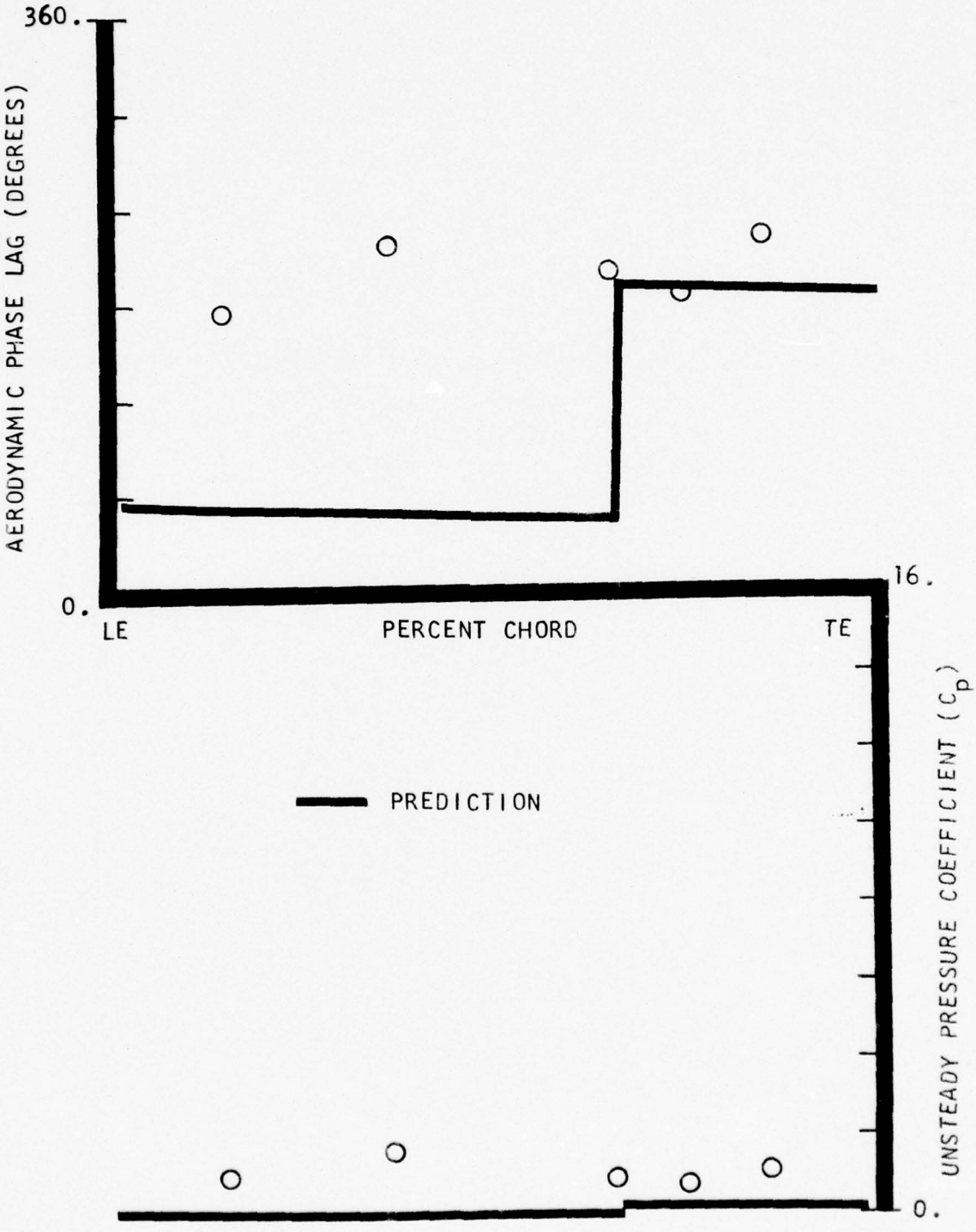


FIGURE 23. CHORDWISE DISTRIBUTION OF THE UNSTEADY CASCADE DATA AND CORRESPONDING FLAT PLATE PREDICTIONS ON THE AIRFOIL PRESSURE SURFACE FOR A -4.4° INTERBLADE PHASE ANGLE AT A STATIC PRESSURE RATIO OF 1.05:1

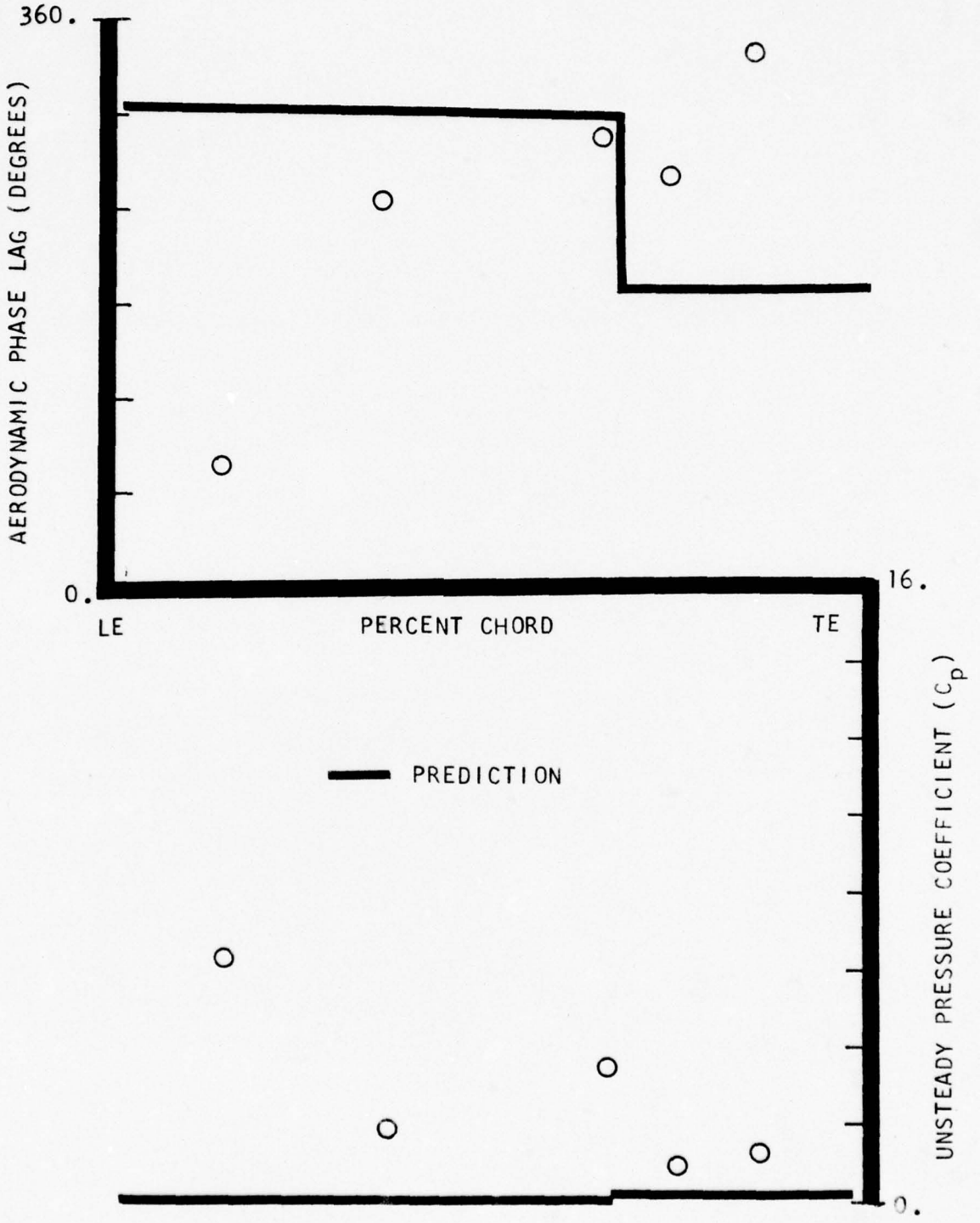


FIGURE 24. CHORDWISE DISTRIBUTION OF THE UNSTEADY CASCADE DATA AND CORRESPONDING FLAT PLATE PREDICTIONS ON THE AIRFOIL PRESSURE SURFACE FOR A 46.6° INTERBLADE PHASE ANGLE AT A STATIC PRESSURE RATIO OF 1.05:1

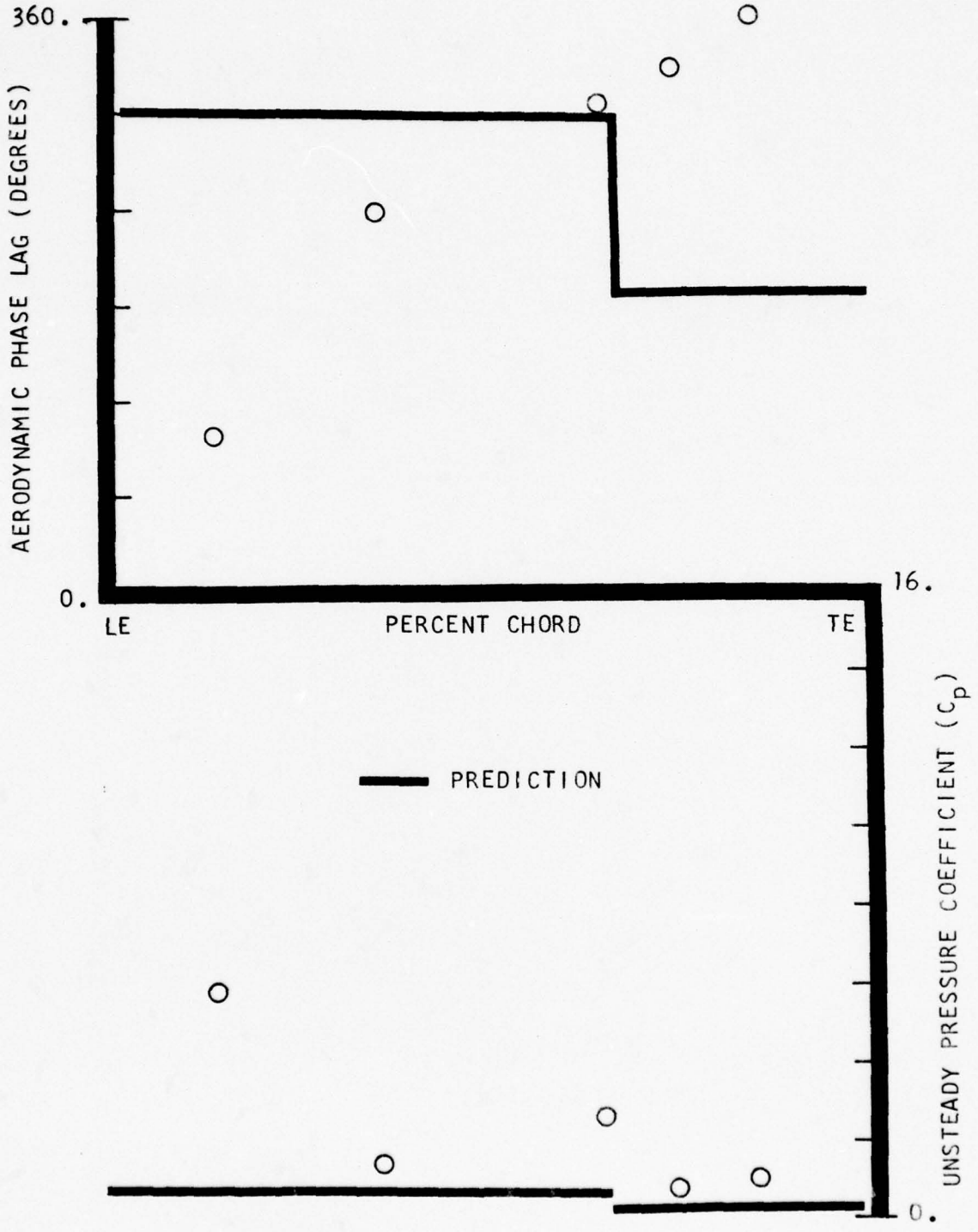


FIGURE 25. CHORDWISE DISTRIBUTION OF THE UNSTEADY CASCADE DATA AND CORRESPONDING FLAT PLATE PREDICTIONS ON THE AIRFOIL PRESSURE SURFACE FOR A 58.2° INTERBLADE PHASE ANGLE AT A STATIC PRESSURE RATIO OF 1.05:1

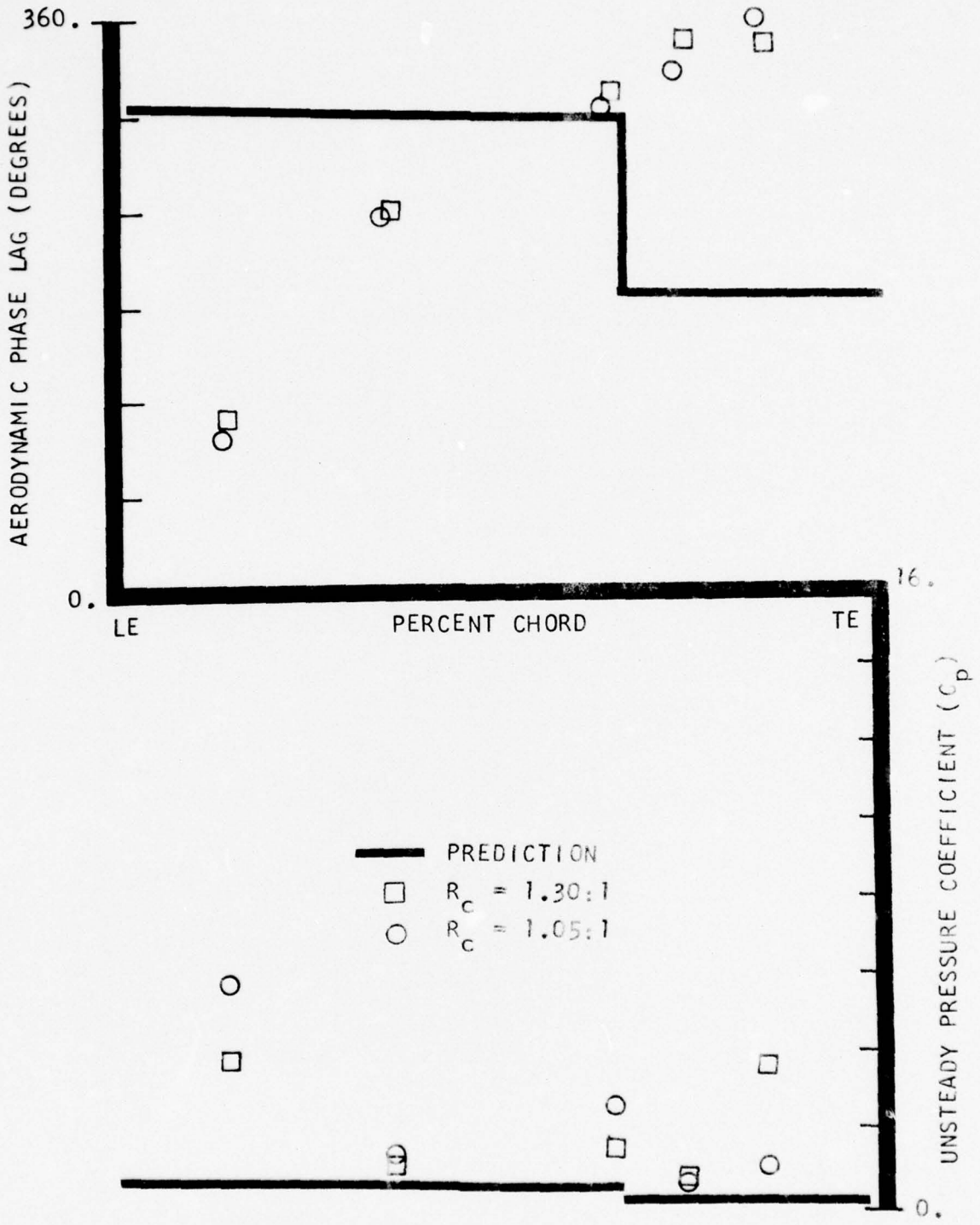


FIGURE 26. CHORDWISE DISTRIBUTION OF THE UNSTEADY CASCADE DATA AND CORRESPONDING FLAT PLATE PREDICTIONS ON THE AIRFOIL PRESSURE SURFACE FOR 56.7° AND 58.2° INTERBLADE PHASE ANGLES AT STATIC PRESSURE RATIOS OF 1.30:1 AND 1.05:1, RESPECTIVELY

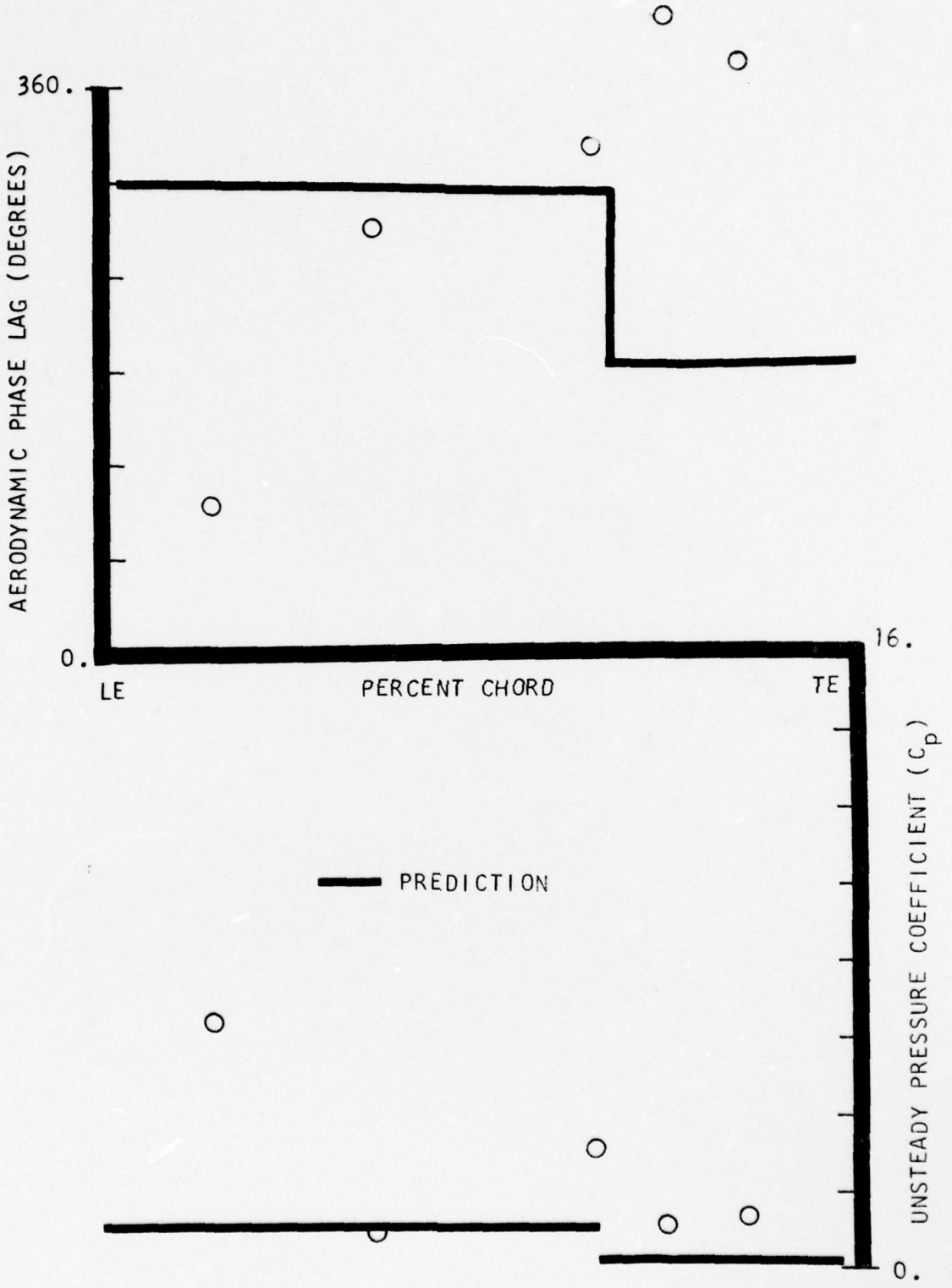


FIGURE 27. CHORDWISE DISTRIBUTION OF THE UNSTEADY CASCADE DATA AND CORRESPONDING FLAT PLATE PREDICTIONS ON THE AIRFOIL PRESSURE SURFACE FOR A 70.2° INTERBLADE PHASE ANGLE AT A STATIC PRESSURE RATIO OF 1.05:1

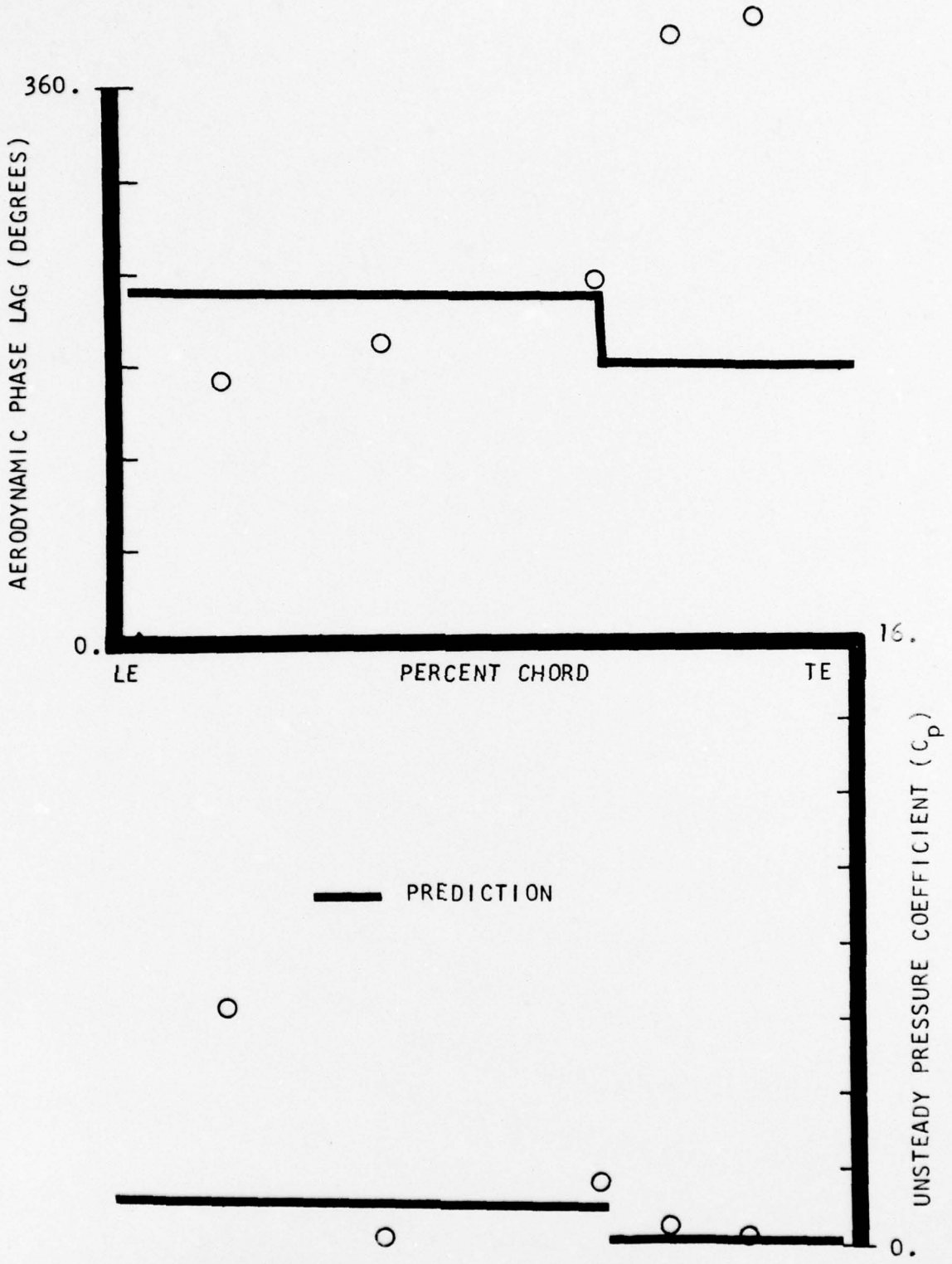


FIGURE 28. CHORDWISE DISTRIBUTION OF THE UNSTEADY CASCADE DATA AND CORRESPONDING FLAT PLATE PREDICTIONS ON THE AIRFOIL PRESSURE SURFACE FOR A 130.6° INTERBLADE PHASE ANGLE AT A STATIC PRESSURE RATIO OF 1.05:1

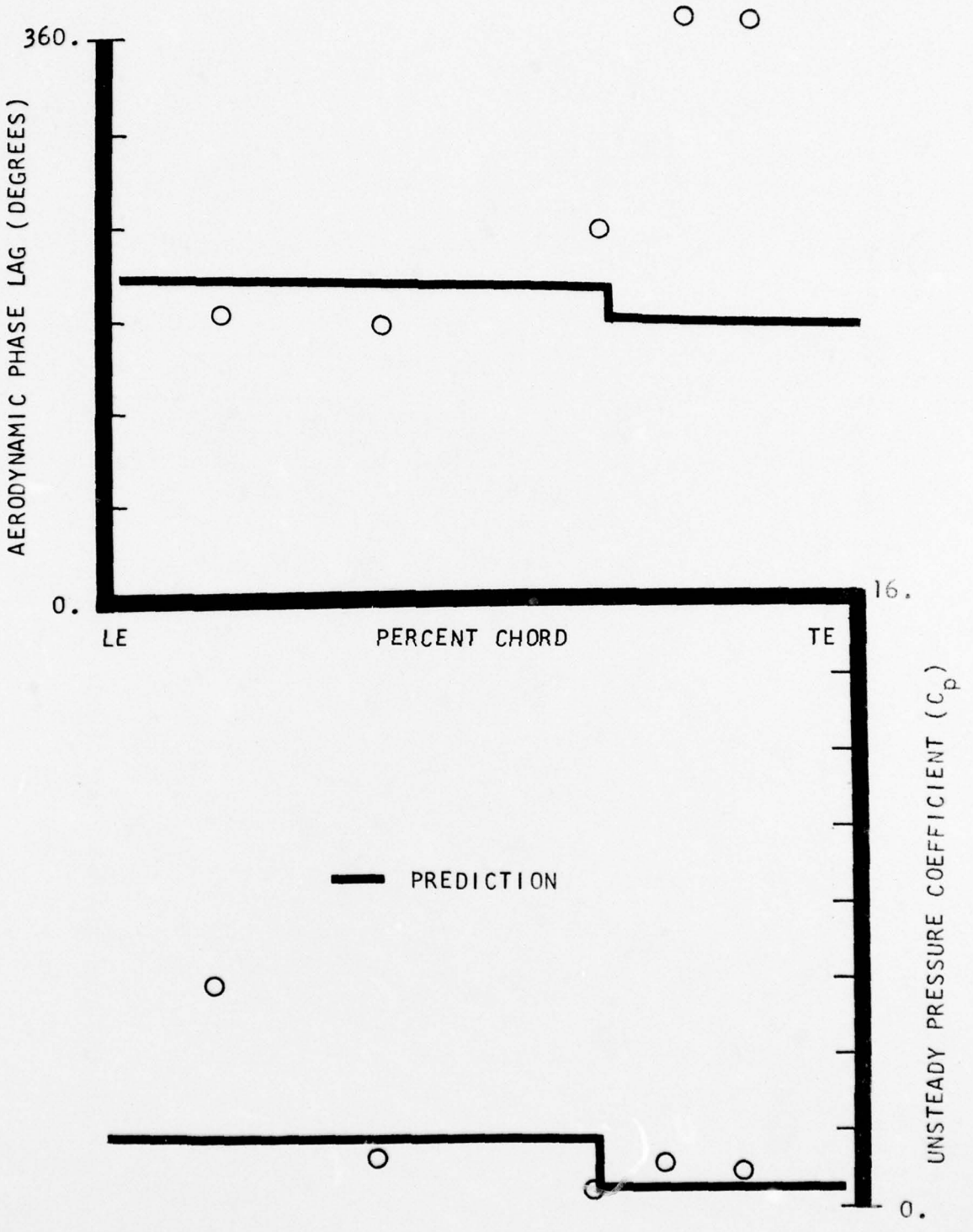


FIGURE 29. CHORDWISE DISTRIBUTION OF THE UNSTEADY CASCADE DATA AND CORRESPONDING FLAT PLATE PREDICTIONS ON THE AIRFOIL PRESSURE SURFACE FOR A 162.1° INTERBLADE PHASE ANGLE AT A STATIC PRESSURE RATIO OF 1.05:1

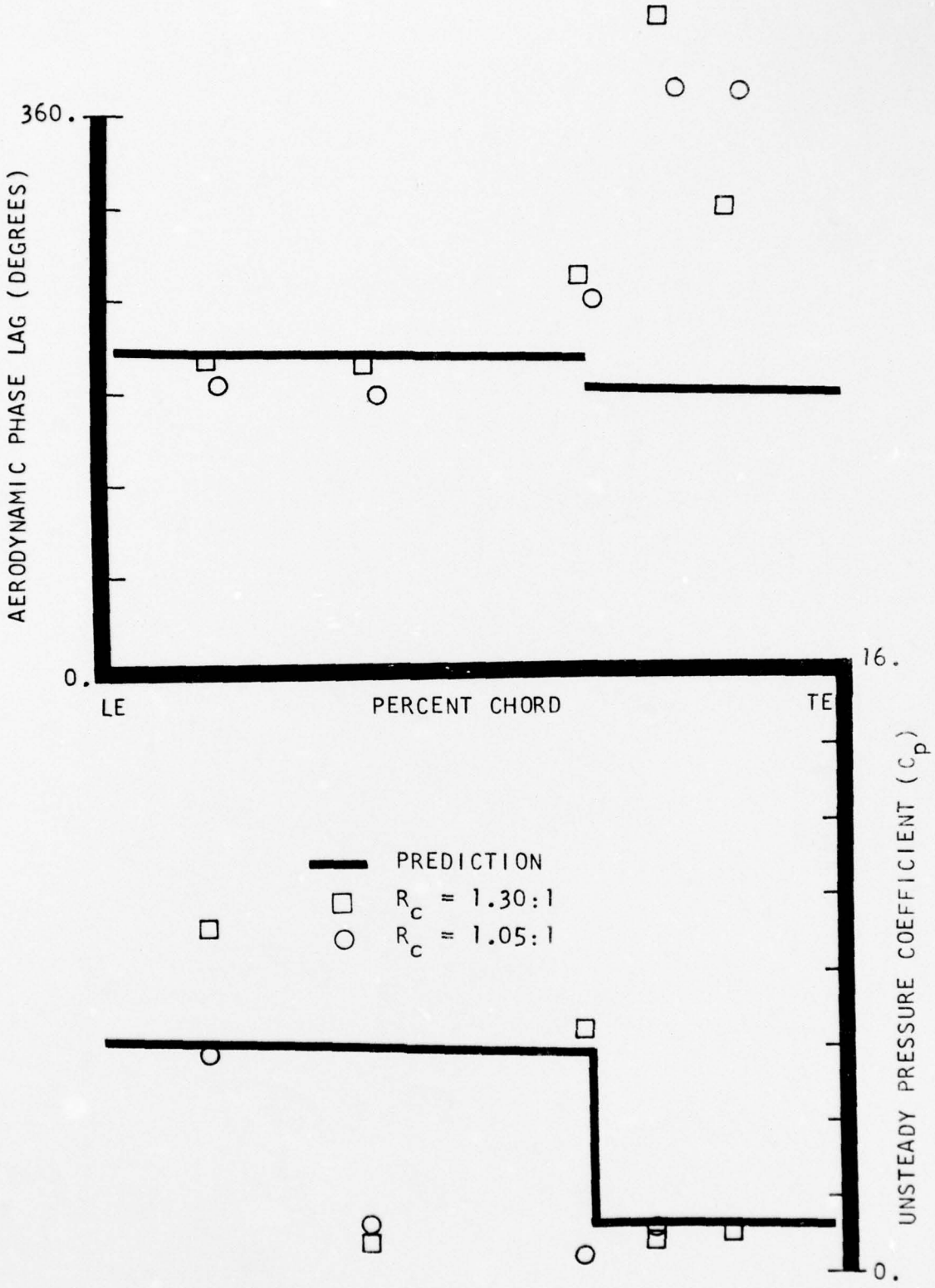


FIGURE 30. CHORDWISE DISTRIBUTION OF THE UNSTEADY CASCADE DATA AND CORRESPONDING FLAT PLATE PREDICTIONS ON THE AIRFOIL PRESSURE SURFACE FOR 163.1° AND 162.1° INTERBLADE PHASE ANGLES AT STATIC PRESSURE RATIOS OF 1.30:1 AND 1.05:1, RESPECTIVELY.

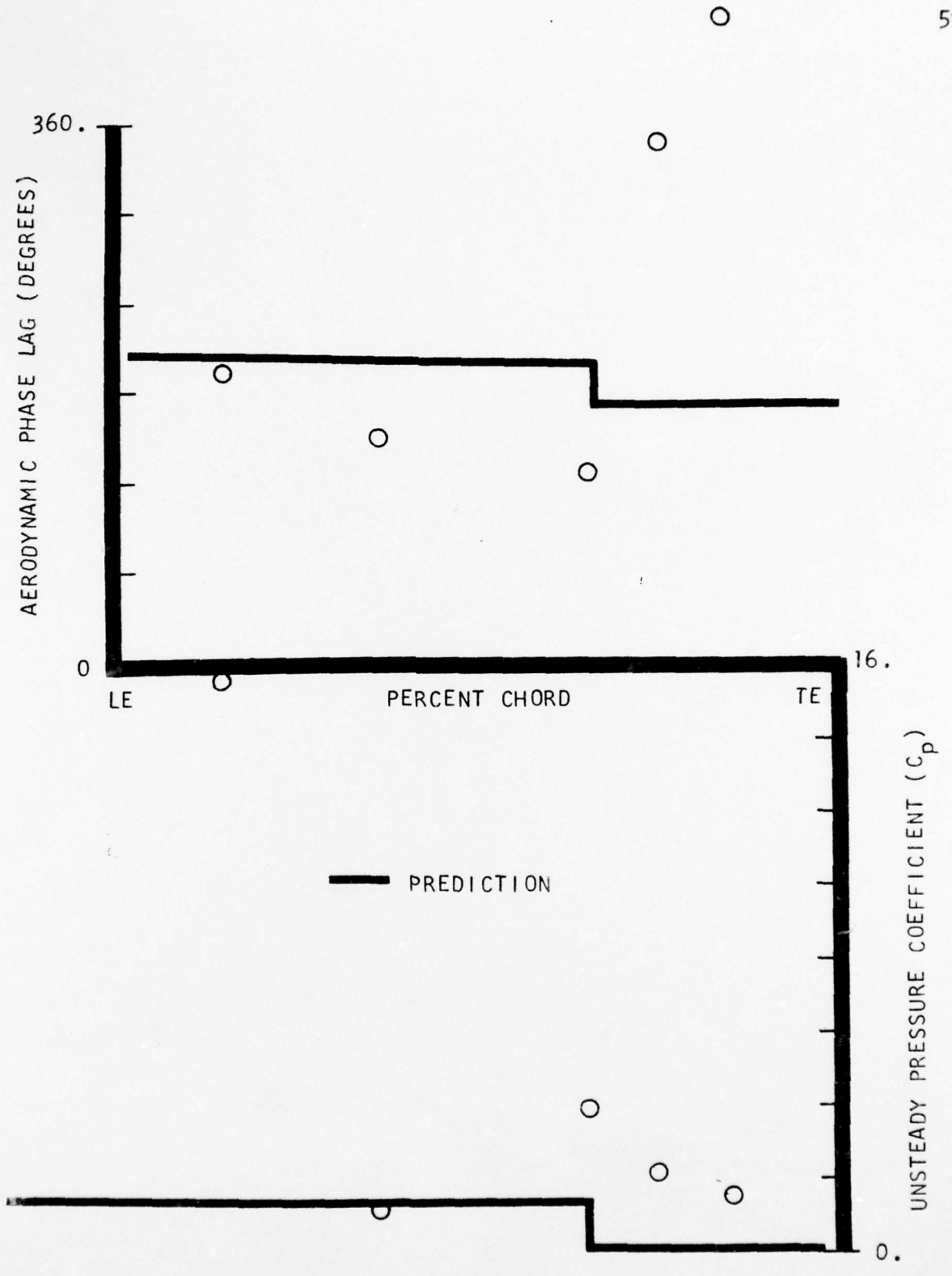


FIGURE 31. CHORDWISE DISTRIBUTION OF THE UNSTEADY CASCADE DATA AND CORRESPONDING FLAT PLATE PREDICTIONS ON THE AIRFOIL PRESSURE SURFACE FOR A 170.2° INTERBLADE PHASE ANGLE AT A STATIC PRESSURE RATIO OF 1.05:1

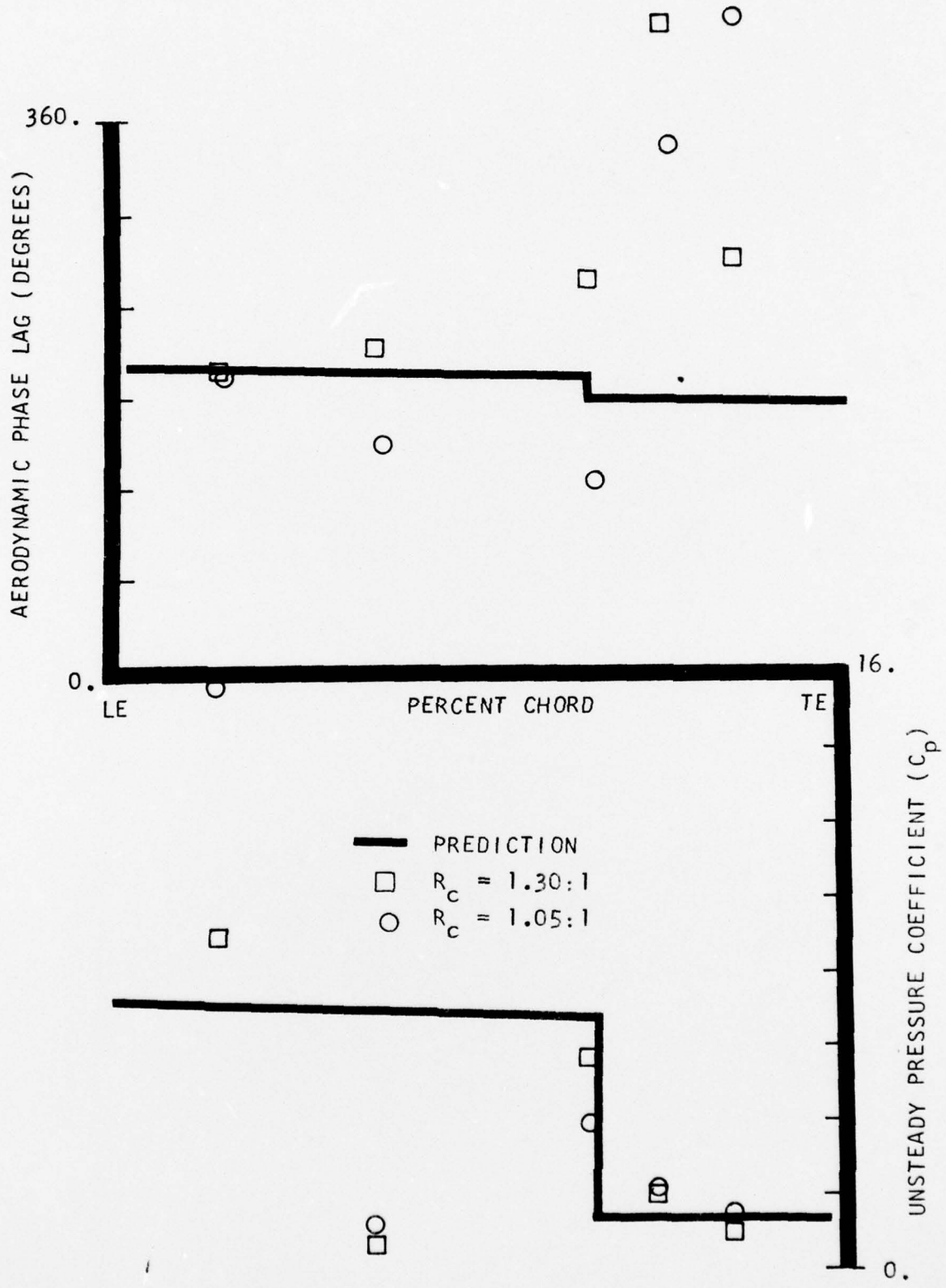


FIGURE 32. CHORDWISE DISTRIBUTION OF THE UNSTEADY CASCADE DATA AND CORRESPONDING FLAT PLATE PREDICTIONS ON THE AIRFOIL PRESSURE SURFACE FOR 173.4° AND 170.2° INTERBLADE PHASE ANGLES AT STATIC PRESSURE RATIOS OF 1.30:1 AND 1.05:1, RESPECTIVELY

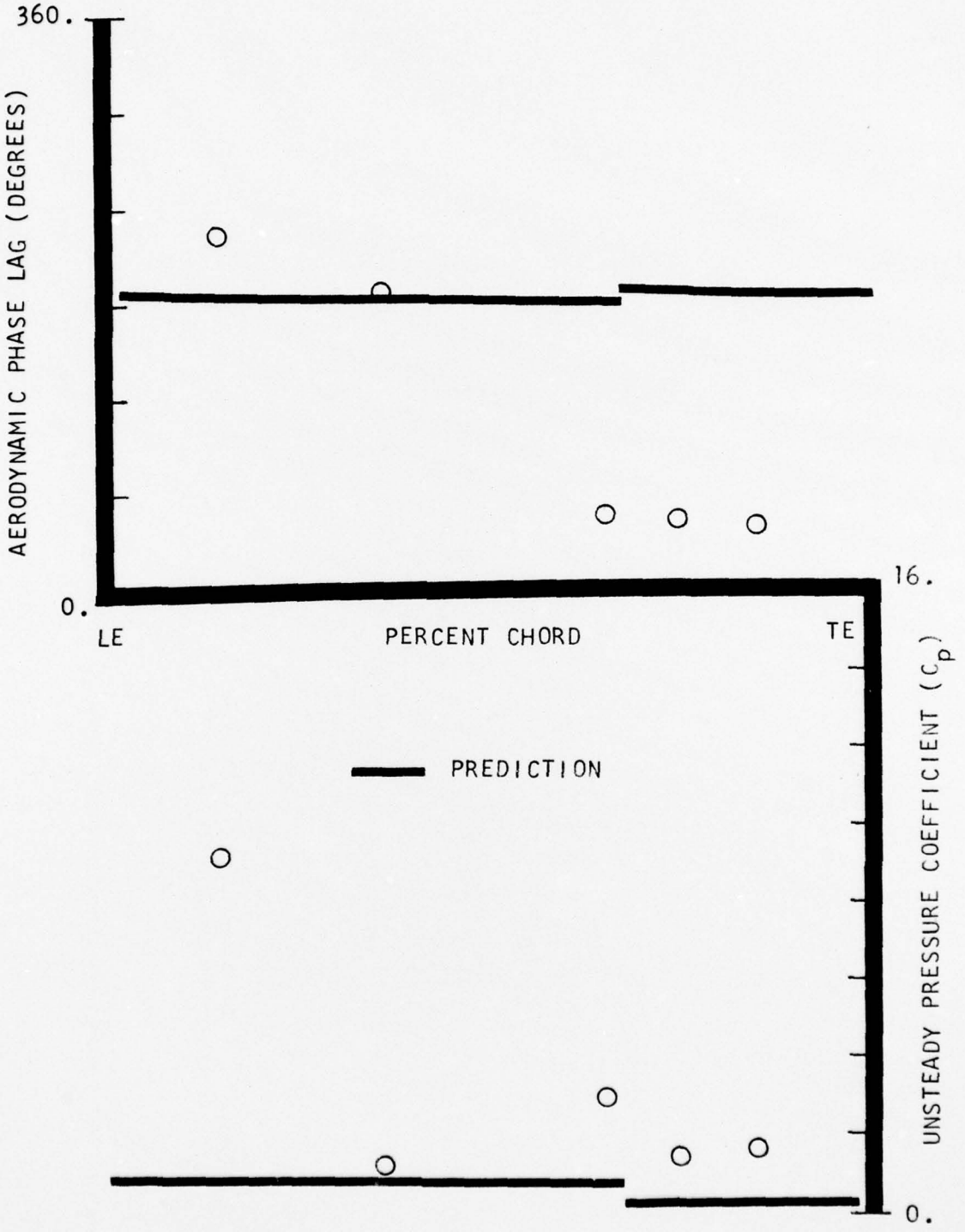


FIGURE 33. CHORDWISE DISTRIBUTION OF THE UNSTEADY CASCADE DATA AND CORRESPONDING FLAT PLATE PREDICTIONS ON THE AIRFOIL PRESSURE SURFACE FOR A 193.8° INTERBLADE PHASE ANGLE AT A STATIC PRESSURE RATIO OF 1.05:1

# REFERENCES

1. Chadwick, W. R., Bell, J. K., and Platzer, M. F., "On the Analysis of Supersonic Flow Past Oscillating Cascades", AGARD-CP-177, Unsteady Phenomena in Turbomachinery, 1975.

2. Fleeter, S., Novick, A. S., and Riffel, R. E., "An Experimental Determination of the Unsteady Aerodynamics in a Controlled Oscillating Cascade", ASME Paper No. 76-GT-47, 1976.

3. Fleeter, S., McClure, R. B., Sinnet, G. T. and Holtman, R. L., "Supersonic Inlet Torsional Cascade Flutter", Journal of Aircraft, Vol. 12, No. 8, August, 1975.

4. Kurzrock, J. W. and Novick, A. S., "Transonic Flow Around Rotor Blade Elements", Journal of Fluids Engineering, Vol. 97, December 1975.

5. Caruthers, J. E., "Theoretical Analysis of Unsteady Supersonic Flow Around Harmonically Oscillating Turbofan Cascades", Ph.D. Thesis, Georgia Institute of Technology, June 1976.

6. Fleeter, S., Novick, A. S., and Riffel, R. E., "The Unsteady Aerodynamic Response of an Airfoil Cascade to a Time-Variant Supersonic Inlet Flow Field", AGARD-CP-177, Unsteady Phenomena in Turbomachinery, 1975.

| Recipient | No. of Copies |
|---|---|
| Director<br>Power Program<br>Material Sciences Division<br>Office of Naval Research<br>Department of the Navy<br>800 North Quincy Street<br>Arlington, Virginia 22217 | (1) |
| Chief of Naval Research<br>Department of the Navy<br>Washington, D.C. 20360<br>Attn: Mr. J. R. Patton, Jr., Code 473 | (1) |
| Director<br>U.S. Naval Research Laboratory<br>Washington, D.C. 20390<br>Attn: Library, Code 2029 (ONRL) | (6) |
| Director<br>U.S. Naval Research Laboratory<br>Washington, D.C. 20390<br>Attn: Technical Information Division | (6) |
| Defense Documentation Center<br>Building 5<br>Cameron Station<br>Alexandria, Virginia 22314 | (12) |
| Commander<br>Naval Air Systems Command<br>Department of the Navy<br>Washington, D.C. 20360 | |
| Attn: Mr. R. R. Brown, Code 53673 | (1) |
| Mr. I. Silver, Code 330 | (1) |
| Dr. H. Rosenwasser, Code 310C | (1) |
| Technical Library Division, Code 604 | (1) |

| Recipient | No. of Copies |
|---|---|
| Commander<br>Naval Ship Systems Command<br>Department of the Navy<br>Washington, D.C. 20360 | |
| Attn: Mr. R. R. Peterson, Code 03413 | (1) |
| Mr. C. Miller, Code 6146 | (1) |
| Technical Library | (1) |
| Commanding Officer<br>U.S. Army Research Office<br>Box CM, Duke Station<br>Durham, North Carolina 27706 | |
| Attn: ORDOR-PC | (1) |
| Director<br>National Aeronautics and Space Administration<br>Headquarters<br>Washington, D.C. 20546 | |
| Attn: Division Research Information | (1) |
| Office of the Assistant Secretary of Defense (R & D)<br>Room 3E1065 - The Pentagon<br>Washington, D.C. 20301 | |
| Attn: Technical Library | (1) |
| General Motors Corporation<br>Allison Division<br>Indianapolis, Indiana 46206 | |
| Attn: Director of Engineering | (1) |
| National Aeronautics and Space Administration<br>Lewis Research Center<br>21000 Brookpark Road<br>Cleveland, Ohio 44135 | (2) |
| Commander<br>U.S. Naval Ordnance Laboratory<br>White Oak<br>Silver Spring, Maryland 20910 | |
| Attn: Library | (1) |

| Recipient | No. of Copies |
|---|---|
| Commander<br>Naval Weapons Center<br>China Lake, California 93555<br>Attn: Technical Library | (1) |
| Commander<br>Wright Air Development Center<br>Wright-Patterson Air Force Base, Ohio 45433<br>Attn: WCLPN-1, WCACD, WCLPS-1 | (3) |
| Officer in Charge<br>Naval Ship Engineering Center<br>Philadelphia Division<br>Philadelphia, Pennsylvania 19112<br>Attn: Code 6700<br>Technical Library | (1)<br>(1) |
| Superintendent<br>U.S. Naval Postgraduate School<br>Monterey, California 93940<br>Attn: Professor Vavra<br>Library, Code 0212 | (1)<br>(1) |
| Commander<br>Naval Ordnance Systems Command<br>Department of the Navy<br>Washington, D.C. 20360<br>Attn: Mr. B. Drimmer, Code 033 | (1) |
| Naval Ship Research and Development Center<br>Annapolis, Maryland 21402<br>Attn: Library, Code A214 | (1) |
| Naval Undersea Warfare Center<br>3202 East Foothill Boulevard<br>Pasadena, California 91107<br>Attn: Technical Library | (1) |
| Naval Applied Science Laboratory<br>Flushing and Washington Avenues<br>Brooklyn, New York 11251<br>Attn: Technical Library, Code 222 | (1) |

| Recipient | No. of Copies |
|---|---|
| Bureau of Naval Personnel<br>Department of the Navy<br>Washington, D.C. 20370<br>Attn: Technical Library | (1) |
| U.S. Naval Weapons Laboratory<br>Dahlgren, Virginia 22448<br>Attn: Technical Library | (1) |
| Director, Project SQUID<br>Jet Propulsion Center<br>School of Mechanical Engineering<br>Purdue University<br>Lafayette, Indiana 47907<br>Attn: Dr. Robert Goulard | (1) |
| Army Missile Command<br>Research and Development Directorate<br>Redstone Arsenal, Alabama 35809<br>Attn: Propulsion Laboratory | (1) |
| Commander<br>U.S. Air Force Systems Command<br>Andrews Air Force Base<br>Silver Hill, Maryland 20331 | (1) |
| Commander<br>Air Force Aero Propulsion Laboratory<br>Wright-Patterson Air Force Base<br>Dayton, Ohio 45433 | (1) |
| Commander<br>Air Force Rocket Propulsion Laboratory<br>Edwards Air Force Base, California 93523 | (1) |
| Naval Missile Center<br>Point Mugu, California 93041<br>Attn: Technical Library<br>Code 5632.2 | (1) |

| Recipient | No. of Copies |
|---|---|
| Headquarters<br>Naval Material Command<br>Special Projects Office<br>Washington, D.C. 20360<br>Attn: Technical Library | (2) |
| Commander<br>Air Force Office of Scientific Research<br>1400 Wilson Boulevard<br>Arlington, Virginia 22209<br>Attn: J. F. Masi<br>M. Rogers | (1) |
| Director of Defense Research and Engineering<br>Technical Library<br>Room 3C128 - The Pentagon<br>Washington, D.C. 20301<br>Attn: Propulsion Technology | (1) |
| Chief of Research and Development<br>Headquarters, Department of the Army<br>Washington, D.C. 20310<br>Attn: Dr. S. J. Magram<br>Physical and Engineering Division | (1) |

Unclassified

SECURITY CLASSIFICATION OF THIS PAGE (When Data Entered)

(14) DDA-EDR-9028

## REPORT DOCUMENTATION PAGE

READ INSTRUCTIONS BEFORE COMPLETING FORM

1. REPORT NUMBER: EDR 9028

2. GOVT ACCESSION NO.

3. RECIPIENT'S CATALOG NUMBER

(6) TITLE (and Subtitle): Research on Aeroelastic Phenomena in Airfoil Cascades; An Experimental Investigation of the Unsteady Aerodynamics of a Controlled Oscillating MCA Airfoil Cascade,

5. TYPE OF REPORT & PERIOD COVERED: (9) Technical Report,

6. PERFORMING ORG. REPORT NUMBER

7. AUTHOR(s): (10) Sanford Fleeter and Ronald E. Riffel

8. CONTRACT OR GRANT NUMBER(s): (15) N00014-72-C-0351

9. PERFORMING ORGANIZATION NAME AND ADDRESS:
Detroit Diesel Allison Division
General Motors Corporation
Indianapolis, Indiana 46206

10. PROGRAM ELEMENT, PROJECT, TASK AREA & WORK UNIT NUMBERS: NR 094-369

11. CONTROLLING OFFICE NAME AND ADDRESS:
Power Branch
Office of Naval Research - Code 473
Arlington, Virginia 22217

12. REPORT DATE: (11) December 1976

13. NUMBER OF PAGES: (12) 79 p.

14. MONITORING AGENCY NAME & ADDRESS (if different from Controlling Office)

15. SECURITY CLASS. (of this report): Unclassified

15a. DECLASSIFICATION/DOWNGRADING SCHEDULE

16. DISTRIBUTION STATEMENT (of this Report)

This document has been approved for public release and sale; its distribution is unlimited.

17. DISTRIBUTION STATEMENT (of the abstract entered in Block 20, if different from Report)

See AD17203

18. SUPPLEMENTARY NOTES

19. KEY WORDS (Continue on reverse side if necessary and identify by block number)

Flutter, Aeroelasticity, Turbomachinery, Aerodynamics, Experimental Techniques, Cascades, Dynamic Measurements

20. ABSTRACT (Continue on reverse side if necessary and identify by block number)

A unique unsteady cascade experiment directed at providing fundamental aerodynamic data needed to verify or direct refinements to the basic model of unstalled supersonic torsional flutter in turbomachines is presented. In particular, the steady, quasi-static, and unsteady aerodynamics were determined for a multiple circular arc (MCA) airfoil cascade which modeled the tip section of an advanced design fan blade. The steady

DD FORM 1 JAN 73 1473 EDITION OF 1 NOV 65 IS OBSOLETE

Unclassified

SECURITY CLASSIFICATION OF THIS PAGE (When Data Entered)

019200

airfoil surface aerodynamic performance of the cascade was measured at two levels of aerodynamic loading and correlated with the predictions from a time-marching, steady, transonic flow analysis. The chordwise distribution of the quasi-static unsteady pressure coefficient for a 0° interblade phase angle was then determined and correlated with two appropriate predictions: one based on the steady transonic analysis and the other on steady inviscid supersonic flat plate theory. Finally, the MCA cascade was harmonically oscillated in the torsional mode at a reduced frequency value of 0.14. The fundamental unsteady aerodynamic data was then obtained at a Mach number equal to 1.55 over a range of interblade phase angles for two values of the cascade static pressure ratio. These unsteady results were then correlated with the predictions from state-of-the-art unsteady flat plate cascade analyses.